TÜBİTAK

Turkish Journal of Earth Sciences

http://journals.tubitak.gov.tr/earth/

Research Article

Turkish J Earth Sci
(2021) 30: 59-80

doi:10.3906/yer-2004-16

Geochemistry and U-Pb ages from the Kösdağ Metavolcanics in the southern Central Pontides (Turkey): Complementary data for early Late Cretaceous island arc development in the Northern Neotethys

Faruk BERBER[1,*], **Kaan SAYIT**[2], **Mehmet Cemal GÖNCÜOĞLU**[2]
[1]Department of Civil Engineering, Atatürk University, Erzurum, Turkey
[2]Department of Geological Engineering, Middle East Technical University, Ankara, Turkey

Received: 19.04.2020 • **Accepted/Published Online:** 19.10.2020 • **Final Version:** 15.01.2021

Abstract: The Kösdağ Metavolcanics (KMs) in the southern Central Pontides are exposed between the İzmir-Ankara-Erzincan Suture Belt in the south and the Sakarya Composite Terrane in the north. They comprise an approximately 40-km-long tectonic unit, bounded by the splays of the North Anatolian Transform Fault in the north and the Kızılca Thrust in the south. The basement of the unit mainly consists of metabasalts, metaandesites, and metarhyolites, with well-developed blastomylonitic textures, which are interlayered by recrystallized pelagic limestone and chert. Late Cretaceous pelagic limestones of the Dikmen Formation disconformably overlie the basement. Geochemically, the KMs exhibit enrichment in Th and La relative to Nb (and Ti), indicating subduction-related magmatic signatures. The KMs are subdivided into two main types, as Type 1 and Type 2, based on their relative Zr-Hf enrichment/depletion features. All of the members of the KMs have a subalkaline nature (Nb/Y = 0.08–0.19 for Type 1; Nb/Y = 0.05–0.13 for Type 2) and display a calc-alkaline affinity. The high Zr/Nb (38.1–52.9 for Type 1, 21.8–41.2 for Type 2), low Zr/Y (4.07–5.25 for Type 1, 1.58–2.44 for Type 2), and Nb/Y (0.08–0.14 for Type 1, 0.05–0.10 for Type 2) signatures of the KMs indicate that they have derived from a depleted source, which has been modified by a subduction component. The laser ablation inductively-coupled plasma mass spectrometry (LA-ICP-MS) U-Pb zircon ages of the metarhyolite samples ranged between 94.64 ± 0.77 Ma and 113.2 ± 2.3 Ma, suggesting the presence of an intraoceanic subduction zone during the early Late Cretaceous within the İzmir-Ankara-Erzincan branch of the Neotethys Ocean in the Central Pontides.

Key words: Central Pontides, early Late Cretaceous, İzmir-Ankara-Erzincan Suture Belt, island arc, Kösdağ Metavolcanics

1. Introduction

Turkey, one of the key areas to understand the geological evolution of the Tethys oceans, is located in the eastern Mediterranean sector of the Alpine-Himalayan orogenic belt. This belt is characterized by distinct oceanic assemblages and continental fragments that are related with the opening and closure of the Tethys Ocean (Şengör and Yılmaz, 1981; Robertson et al., 1996; Göncüoğlu et al., 1997; Okay and Tüysüz, 1999). During the Mesozoic, the main continental microplates were separated by the Neotethyan oceanic strands. These strands are now represented from the north to south by the Intra-Pontide Suture Belt (IPSB; e.g., Göncüoğlu et al., 2000), the İzmir-Ankara-Erzincan Suture Belt (IAESB), and the SE Anatolian Ophiolite Belt (e.g., Göncüoğlu, 2010) (Figure 1a).

In the Central Pontides, the IPSB, IAESB, and intervening Sakarya Composite Terrane (SCT) can be studied along a narrow traverse of about 40 km (Figure 1a). Each of these suture belts comprises, in addition to ophiolitic bodies and mélange complexes, variably metamorphosed volcanic-volcanoclastic bodies of diverse tectonomagmatic settings that formed during different stages of their oceanic evolution. Hence, for a reconstruction of the regional geodynamic evolution, it is of crucial importance to understand the original paleogeographic and tectonic positions, as well as the age of these volcanic-volcano- clastic bodies.

The Kösdağ Metavolcanics (KMs, Kösedağ Metavolcanics in Berber et al. (2014), which are the main topic of this study, are one of these variably deformed and metamorphosed felsic-intermediate volcanic bodies (e.g., Yaylaçayı Volcanics, Mudurnu Volcanics, Boyalı Volcanics, and Tafano Volcanics) in the southern Central Pontides. Due to the similarities between their rock-types, basement-cover relations, and lithostratigraphy, it is hard

* Correspondence: farukbr@atauni.edu.tr

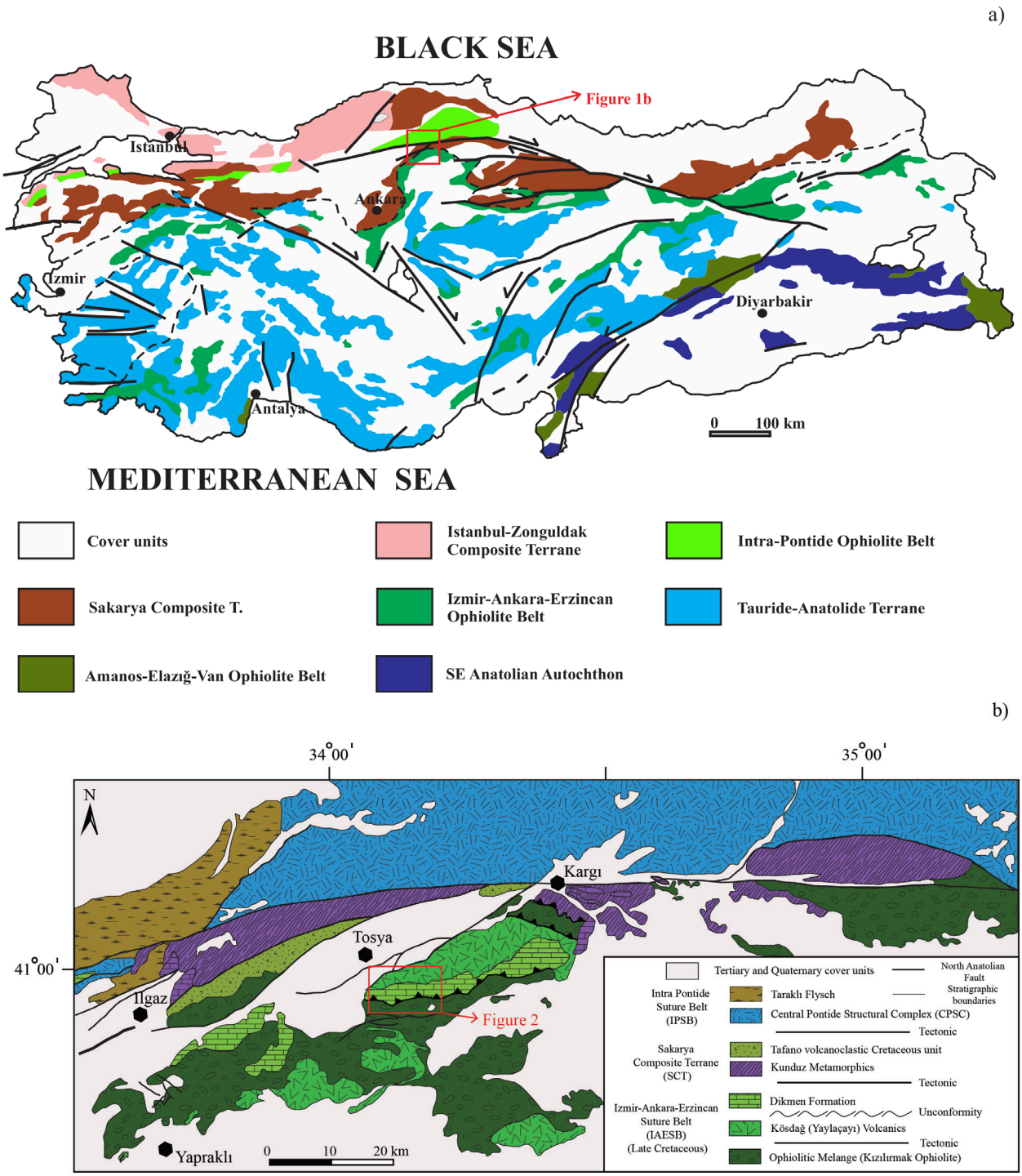

Figure 1. a) Distribution of the main Alpine terranes in northern Turkey (modified from Göncüoğlu, 2010). b) Distribution of the main tectonic units of the Central Pontides.

to distinguish these units in the field without reliable age data. Moreover, the structural relations of these volcanic bodies with the neighboring main tectonic units are obscured by important thrusts, or by the North Anatolian Transform Fault, which runs through the southern Central Pontides and has numerous splays. Hence, a correlation of these units, although very important for the geodynamic evolution of this area, has been a matter of debate. The Yaylaçayı, Mudurnu, Boyalı, and Tafano volcanic units have been relatively well-documented in previous studies

(Tüysüz et al., 1995; Genç and Tüysüz, 2010; Çakıroğlu et al., 2013; Ellero et al., 2015b). However, detailed studies on the geochemistry, tectonomagmatic features, and radiometric age of the KMs are not available. Berber et al. (2014) first published the geochemistry of the KMs. However, they speculated the age of volcanism as Early Jurassic based on the findings of previous studies (e.g., Yılmaz and Tüysüz, 1988). Later, Aygül et al. (2015) provided additional geochemical data and, although limited in number, the first reliable radiometric ages. In this paper, results including a detailed geological map (Figure 2), and more extensive geochemical and geochronological data from the different rock-units of the KMs, to interpret their geological evolution, were presented. In light of the data obtained in this study, and that of previous studies, it was aimed to provide some contribution to the understanding of the evolution of the İzmir-Ankara-Erzincan (IAE) branch of the Neotethys Ocean.

2. Regional geological framework

The Central Pontides comprise a crucial area where representatives of all three main tectono-stratigraphic entities of northern Turkey (IPSB, SCT, and IAESB) juxtapose along the active splays of the North Anatolian Fault in a narrow area (Figure 1a) (e.g., Göncüoglu, 2019).

The geology and geodynamic evolution of the IPSB, immediately to the north of the studied KMs, has recently been studied in detail (Yılmaz et al., 1997; Okay et al., 2013; 2018; Marroni et al., 2020, and the references therein). This belt was formed by the closure of the Intra-Pontide Ocean (IPO) that was opened in the Middle Triassic period (Göncüoğlu et al., 2008; 2012; Tekin et al., 2012) and closed prior to the Early Eocene (Ottria et al., 2017; Marroni et al., 2020). The remnants of this oceanic basin were recently named the Central Pontide Structural Complex (Tekin et al., 2012). From a number of imbricated tectonic units (for details see Frassi et al., 2016; Marroni et al., 2020), only the Arkot Dağ Mélange (Göncüoğlu et al., 2014) and Aylı Dağ Ophiolite (Göncüoğlu et al., 2012) are located immediately at the northern boundary of the KMs (Figure 1b).

The SCT (corresponding to the Sakarya Continent of Şengör and Yılmaz, 1981) is the intervening continental composite terrane between the IPSB and IAESB. It is composed of a Paleozoic basement complex (e.g., Ustaömer and Robertson, 1997; Göncüoğlu et al., 2000; Okay et al., 2006) and its Permian cover (e.g., Göncüoğlu et al., 2004), remnants of a Permian ophiolite (Topuz et al., 2018), and an Early Mesozoic subduction-accretion prism (the Karakaya Complex sensu—Okay and Göncüoğlu, 2004; Sayıt and Göncüoğlu, 2009; 2013), which were accreted during the Late Triassic events (Cimmerian event sensu Şengör and Yılmaz, 1981). The Early Jurassic-Late Cretaceous cover of the SCT represents a south-facing passive margin facing the IPO.

In the Central Pontides, the representatives of the SCT were either thrusted over or juxtaposed by the KMs (e.g., Ellero et al., 2015a) along the North Anatolian Fault Zone (Figure 1b). They occur as lens-shaped bodies around Ilgaz, Tosya, and Kargı (e.g., Ellero et al., 2015a), surrounded by strands of the North Anatolian Fault (Figure 1b). Yılmaz and Tüysüz (1988) used the name Kunduz Metamorphics for the metamorphic units to the NW of Kargı. The structural relations of the Kunduz Metamorphics with the surrounding tectonic units are well exposed in the SW of Kargı, where metaclastics, metabasics, and marbles of the former were thrusted onto the ophiolites of the IAESB. Overall, the SCT comprises metavolcanic-metaclastic rocks dominated by intercalations of calc-schists, quartzofeldspathic schists, and blocks of recrystallized limestones. The metavolcanic rocks are mainly alkali-basalts and andesites. Relict igneous phases in the metavolcanics are clinopyroxene and sphene. Metamorphic minerals are albite, epidote, Na-amphibole, and chlorite. Metaclastic rocks are metagraywackes that include chlorite, Na-amphibole, epidote, albite, and actinolite. White mica, quartz, plagioclase, and epidote occur as metamorphic phases in the quartzofeldspathic schists. Less abundant lithologies are black slates and Na-amphibole-bearing calc-schists. The limestone blocks may vary in size, from a few meters to several hundred meters, and are made up of coarse-grained calcite. This basement is correlated with the Triassic Karakaya Complex elsewhere in the SCT (Tüysüz et al., 1995; Okay and Göncüoğlu, 2004; Sayıt and Göncüoğlu, 2009; 2013; Sayit et al., 2011). This basement is disconformably overlain by red metaconglomerates, metasandstones, and slates, followed by a thick package of gray to pink recrystallized limestones. The upper part of the cover is represented by beige-marly limestones (Soğukçam Limestone) of Albian-Cenomanian age (e.g., Catanzariti et al., 2013). They grade into the turbidites and turbiditic sandstones of the Taraklı Flysch (Yapraklı Formation of Tüysüz et al., 1995). Within the upper part of the turbidites, Ellero et al. (2015b) recently reported continental arc-type basaltic to basaltic-andesite lavas and volcaniclastics (Tafano Volcanics) of Santonian-Campanian age. The deposition of the turbidites lasted through the Late Cretaceous-Paleocene transition and is unconformably overlain by Early Eocene sediments (Ottria et al., 2017).

The third main tectonic unit in contact with the studied KMs is the IAESB. Regionally, it extends between the SCT and the Anatolide-Tauride microcontinent. This suture belt includes remnants of the IAE branch of the Neotethys Ocean that closed by multiple northward-directed subduction zones, comprising a northern one beneath the

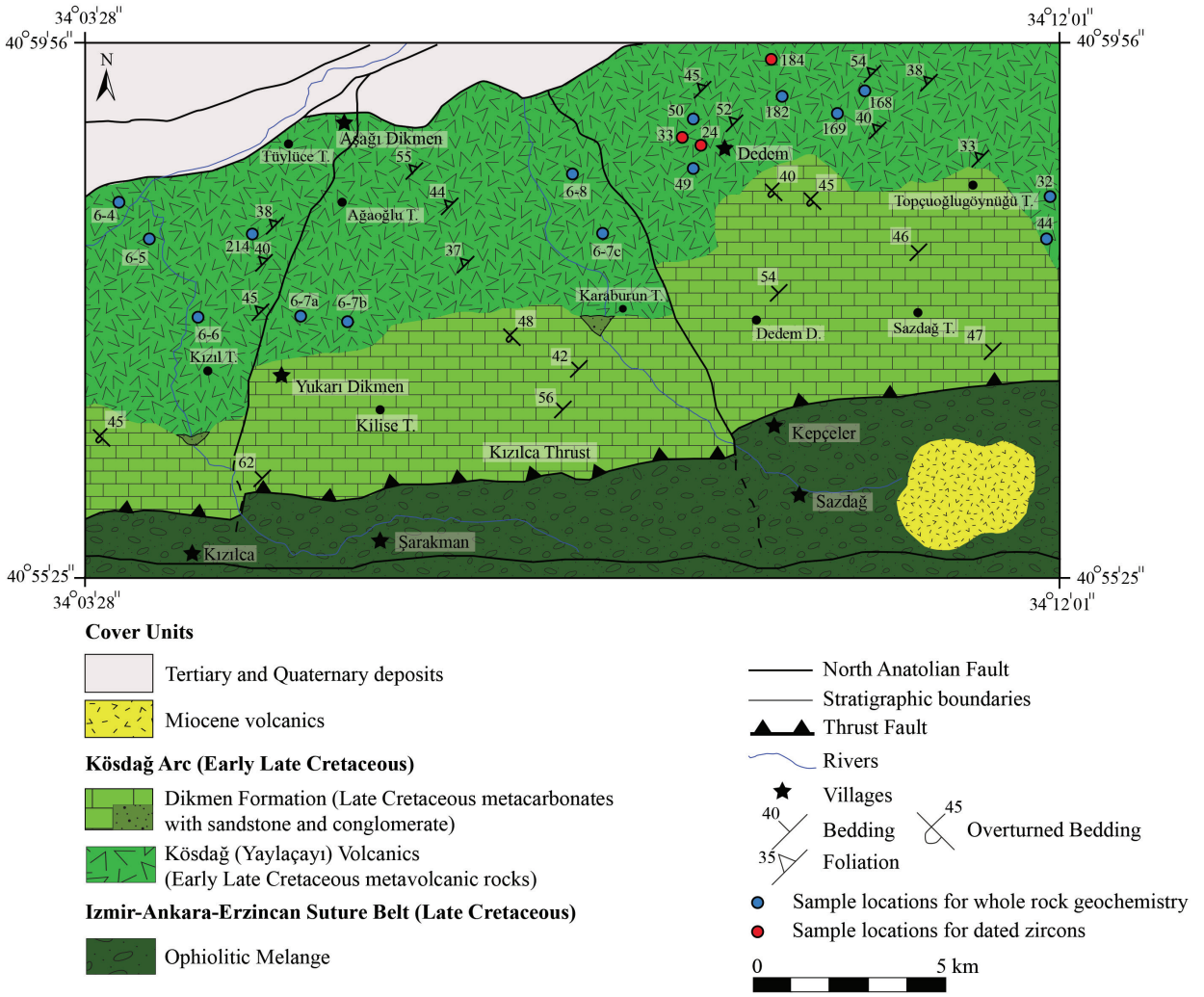

Figure 2. Geological map of the study area.

SCT, and a southern and intra-oceanic one creating the supra-subduction zone-type ophiolites within the suture belt, as early as the Middle Jurassic (e.g., Göncüoğlu et al., 2010; Çelik et al., 2011; Sayit et al., 2016). To the south of the Kös Dağ ridge, the IAESB is represented by the Kızılırmak Ophiolitic Mélange (Tüysüz, 1990). It signifies the northernmost part of the Ankara Mélange, and crops out as a continuous belt in the north of the Çankırı Basin (Figure 1b). The contact relationship between the carbonate cover (Dikmen Formation) and the ophiolitic mélange is a steep reverse fault (Kızılca Thrust) in the southern part of the study area. In the SW, around Kızılca Village, the contact between the Dikmen Formation and the mélange is a thrust fault. The ophiolitic mélange consists of slide-blocks of serpentinized harzburgite, cumulate pyroxenite, dunite, isotropic and layered gabbro, radiolarian chert, and deformed greenschist facies metabasaltic pillow lava in a clastic matrix. Representatives of the Kızılırmak Ophiolite also crop out in the NE of the study area, in Bayat and Eldivan villages, and along the Kızılırmak River in Pelitcik village, SW of Kargı (Figure 1b), where the ultramafic rocks were thrusted onto the carbonates of the Dikmen Formation. The presence of Campanian-Maastrichtian pelagic fauna (Tüysüz, 1990), from the pelagic limestones interbedded with basaltic pillow lavas, suggests a Late Cretaceous formation age for the Kızılırmak Ophiolitic Mélange.

3. Geological features of the Kösdağ Metavolcanics

The KMs [also named the Kösdağ Metamorphics by Yılmaz and Tüysüz (1988), Kösedağ Metavolcanics by Berber et al. (2014), and Kösdağ Arc by Aygül et al. (2015)] are characterized by metavolcanic rocks consisting of metabasalts, metaandesites, and metadacites, which have been subjected to low-grade metamorphism and a variable degree of mylonitic deformation. Owing to the extensive

neotectonism in the region, the primary relations within these lithologies have largely been destroyed. The dynamic metamorphism is typical for the rocks of the KMs, which distinguishes them from the other metamorphic units of the region. The KMs are bounded from the north by an active splay of the North Anatolian Shear Zone (Figure 2). The effect of faulting is evidenced by the occurrence of shear zones in which the metavolcanic lithologies have been heavily mylonitized. In the study area, the volcanic members of the KMs display cross-cut relationships. In some places, metadacites cut the metabasalts, whereas in other places, metabasalts cut metadacites. Apart from volcanic and subvolcanic rocks, which form the bulk of the KMs, volcaniclastic and sedimentary lithologies interbedded with metavolcanic rocks are also found. The sedimentary lithologies are represented by purple chert and mudstone with ghost radiolarians (Figure 3), indicating a deposition below the carbonate compensation depth.

In previous studies, there has been no consensus on the formation age of the KMs. On the basis of fossil data from the overlying Yaylacık Formation, Hakyemez et al. (1986) suggested a deposition throughout the Malm-Neocomian. Yılmaz and Tüysüz (1988) proposed a Liassic or pre-Liassic age for the formation of the KMs, whereas Tüysüz (1990) suggested formation in the Late Mesozoic. Berber et al. (2014) adopted a Lower-Middle Jurassic age for the volcanism based on the previous studies. The first reliable geochronological data (Aygül et al., 2015) suggested a Late Cretaceous (93.8 ± 1.9 and 94.4 ± 1.9 Ma) formation age for the KMs, which will be evaluated in detail in the following chapters.

The oldest cover unit on the KMs with primary depositional contact is the Dikmen Formation (Tüysüz, 1990). It is represented by slightly metamorphosed yellowish-light grey to pinkish carbonates (Figure 3), alternating with clayey to sandy carbonates, light pinkish mudstones with bands, and lenses of cherts. The formation disconformably overlies the KMs. The ages proposed in previous studies have ranged from the Upper Jurassic-Lower Cretaceous (Hakyemez et al., 1986)[1] to the Cenomanian (Tüysüz, 1990; 1993).

Younger units in contact with the KMs and their cover are the Eocene volcanics exposed to the southeast of the study area and the Miocene volcanics located to the southwest of the Kös Dağ (Sevin and Uğuz, 2011).

4. Petrography

The KMs have been variably affected by postmagmatic processes, such as hydrothermal alteration, metamorphism, and deformation. Petrographically, three groups of metavolcanic lithologies could be identified, comprising metabasalts, metaandesites, and metadacites.

The metabasalts were dark green due to the primary and secondary mineral phases, such as chlorite, epidote, and rare actinolite. Both massive and foliated types were present. A porphyritic texture was prevalent. The primary mineral constituents of the metabasalts were plagioclase and clinopyroxene (Figures 4a and 4b). The plagioclase generally displayed subhedral to euhedral outlines and occurred as both phenocrysts and microlites in the groundmass. Plagioclase formed a seriate texture in some places and was variably altered to sericite and epidote. Clinopyroxene, another prominent constituent of the metabasalts, was also present as phenocrysts and small crystals in the groundmass. It formed a glomeroporphyritic texture in places and was changed to chlorite and epidote. Opaque minerals were magnetite- or pyrite-based on the cubic outlines. Epidote, chlorite, sericite, and calcite represented the typical secondary mineral assemblage in the metabasalts. Actinolite was also present in this assemblage in some places.

The metaandesites were varicolored, exhibiting greenish and dark-greyish colors in the hand specimen. They largely included foliated and, to a lesser extent, nonfoliated varieties. They were hypocrystalline to holocrystalline in their original status. Plagioclase was a major constituent of the metaandesites and occurred as subhedral to euhedral crystals (Figures 4c and 4d). Some plagioclases exhibited concentric zoning. In addition, it was observed as porphyroclast in some samples, which developed after ductile deformation. Sericite, chlorite, and epidote constituted the common metamorphic mineral phases in the metaandesites. The groundmass consisted of fine-grained epidote, plagioclase, and chlorite.

In the hand specimen, the metadacites were generally white in color. They were porphyritic with visible, large grains of K-feldspar, plagioclase, quartz and showed foliation similar to the metaandesites and metabasalts. The main primary constituents of the metadacites were quartz, plagioclase, and to a lesser amount, K-feldspar. Quartz and K-feldspar were found as porphyroclasts enveloped by sericite, implying a mylonitic texture (Figures 4e and 4f). No primary mafic phase existed in the metadacites; all were replaced by chlorite and epidote. Plagioclase was mostly found as subhedral to anhedral crystals, which sometimes occurred as porphyroclasts. Relatively less altered plagioclase grains displayed polysynthetic twinning. Zircon occurred as an accessory phase. The metamorphic mineral assemblage in the metadacites comprised chlorite, epidote, sericite, and calcite.

Apart from these lithologies, volcaniclastics and sedimentary lithologies, including purple radiolarian cherts and mudstones, which were interbedded with the metavolcanics, were also present (Figure 3). The volcaniclastic lithologies were represented by the existence of mineral and volcanic rock fragments. In some places,

[1] Yapraklı, Ilgaz, Çankırı, Çandır Dolayının Jeolojisi. MTA Report, No: 7966

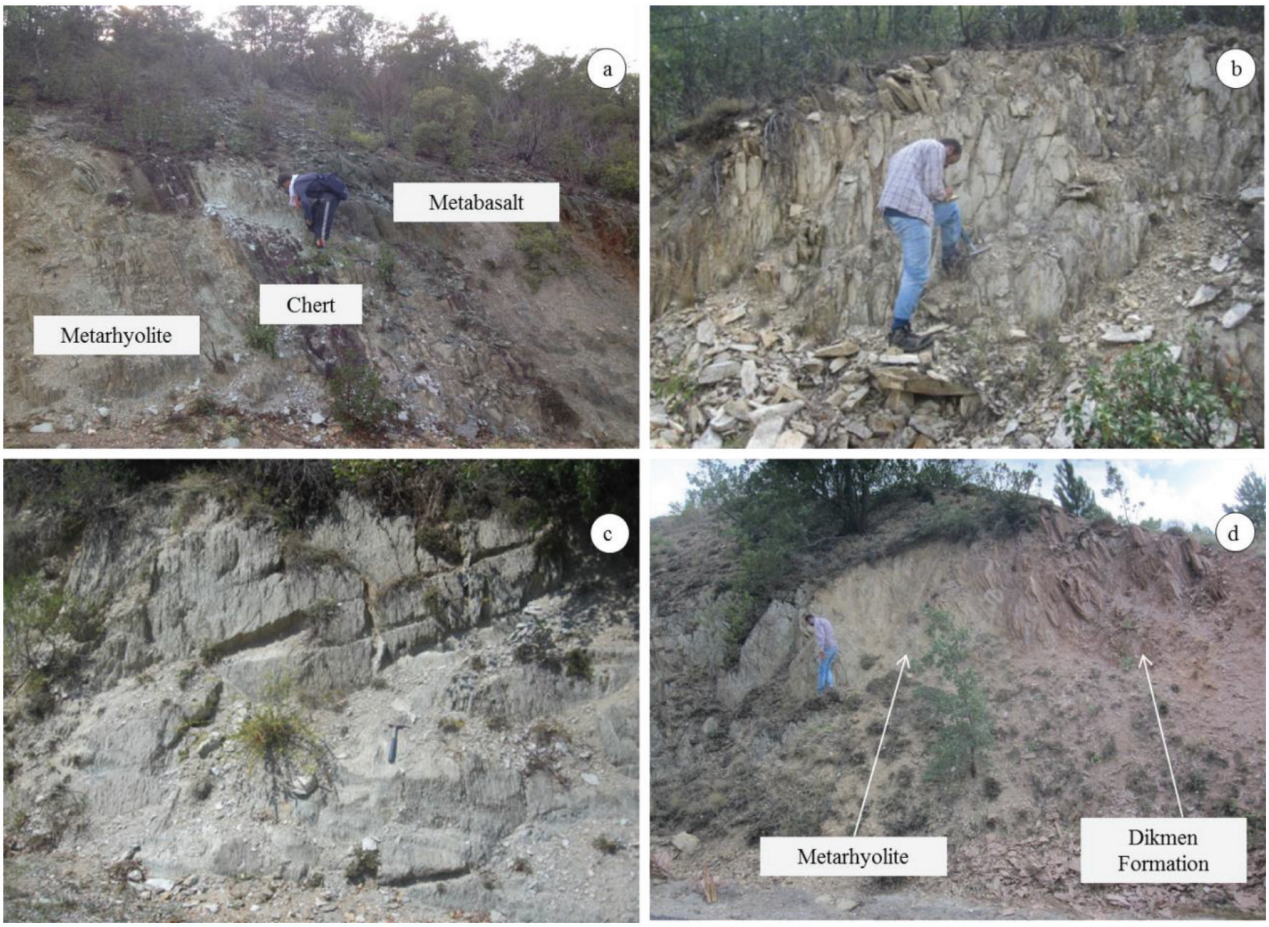

Figure 3. a) KMs alternating with reddish chert interlayers. b) Light-colored meta-dacites with well-developed foliation observed on the road to Yukarıdikmen Village. c) Field photograph of the typical greenish foliated metaandesite. d) Disconformable contact relationship between the KMs and Dikmen Formation cover in northern Kızılca.

sedimentary lithologies outcropping on the main road leading to Yukarıdikmen Village, were observed as bands. Pinkish mudstones included chert nodules in some places.

5. Analytical techniques

A total of 15 rock samples were selected for major and trace element geochemistry. The whole-rock geochemical analyses of the KMs were performed at ACME Analytical Laboratories Ltd. (Vancouver, Canada). For all of the elements, except for Pb and Ni, the samples were fluxed with lithium metaborate/tetraborate and then digested with dilute nitric acid. Concerning Ni and Pb, the samples were digested with aqua regia. Major elements and Sc were determined by inductively-coupled plasma optical emission spectrometry (ICP-OES), whereas the rest of the trace elements [including the rare earth elements (REEs)] were measured using ICP-mass spectrometry (ICP-MS). Loss on ignition was determined by the weight difference after ignition at 1000 °C. Total iron was measured as Fe_2O_3. The geochemical data are presented in Table 1.

U-Pb zircon dating was performed on metarhyolites of the KMs to reveal the crystallization age of the unit. Zircons were separated from metarhyolite samples (24, 33, and 184) at İstanbul Technical University. Measurements were performed using laser ablation-ICP-MS (LA-ICP-MS) at Trinity College in Dublin. The samples investigated, each ~10 kg in weight, were crushed and sieved, and the zircons were separated from the samples using the conventional heavy liquid (sodium polytungstate) and magnetic procedure. The samples were embedded into epoxy mounts and surface polished to expose an equatorial section through the crystals. Zircon 91500 (IAGEO Ltd., Nottingham, UK) was used as the primary standard. Ages and errors were calculated based on the Isoplot 3 macro reported by Ludwig (2003).

6. Results

6.1. Whole rock major and trace elements

The analysed samples are subdivided into two chemical types, as Type 1 and Type 2, based on their relative Zr-

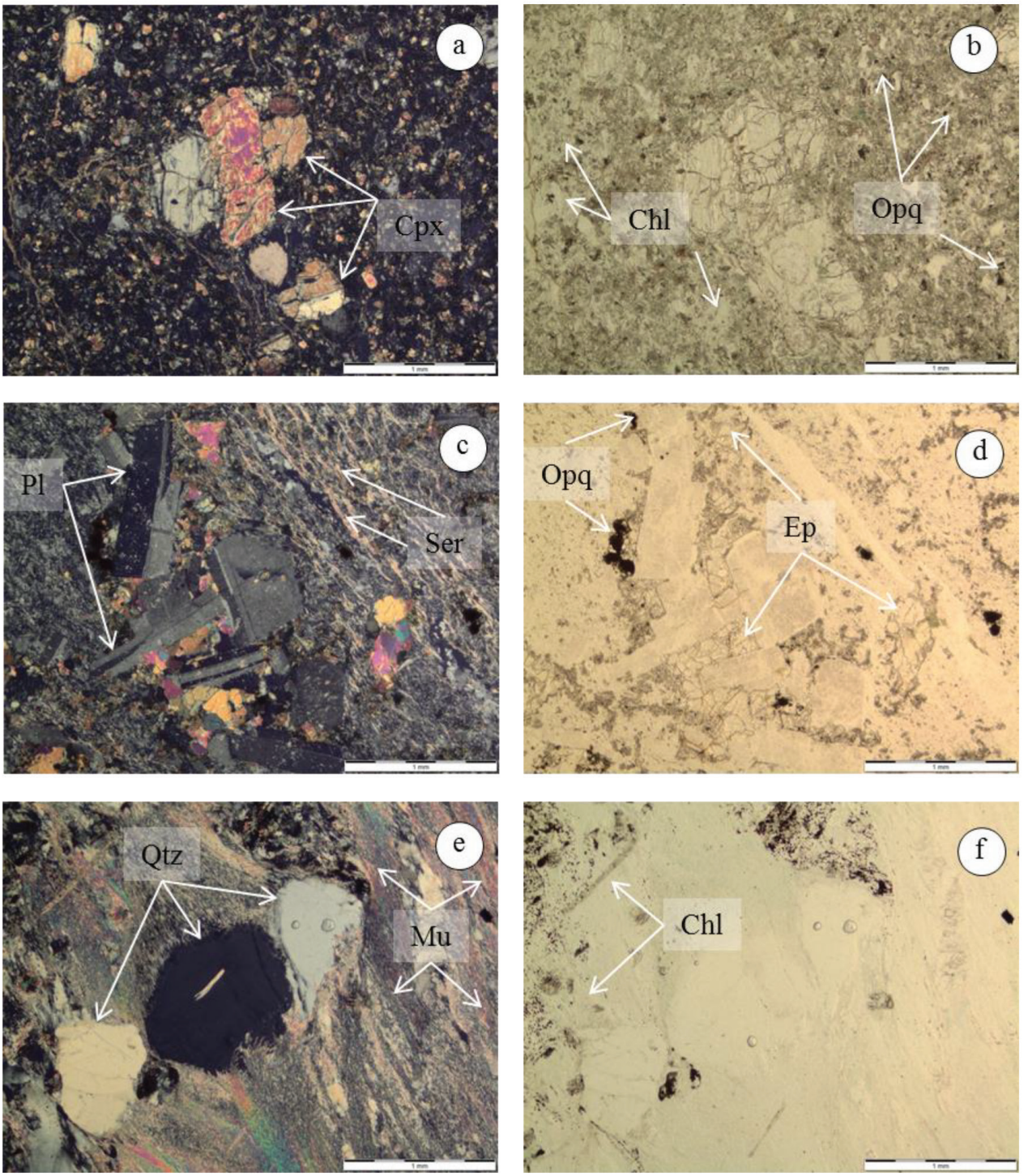

Figure 4. a-b) Photomicrographs of fractured clinopyroxene phenocrysts forming glomeroporphyritic texture in metabasalt. The fine-grained matrix is composed of epidote, chlorite and clinopyroxene. c-d) Plagioclase clusters and groundmass consisting of chlorite and epidote in metaandesite. e-f) Blastomylonite formed by intense deformation of the metadacite, showing aligned white mica adjacent to quartz porphyroclasts. cpx: clinopyroxene, chl: chlorite, opq: opaque, plg: plagioclase, ser: sericite, qtz: quartz, mu: muscovite.

Hf enrichment/depletion. Type 1 showed no relative Zr-Hf depletion over Nd and Sm, whereas Type 2 was depleted of Zr-Hf. The Zr/TiO_2 vs. Nb/Y diagram showed that both types exhibited subalkaline affinity (Nb/Y = 0.08–0.19 for Type 1; Nb/Y = 0.05–0.13 for Type 2). Type 1 rocks appeared to be more felsic in general and

Table 1. Major and trace element compositions of investigated samples from the KMs.

	6–4	6–5	6–6	6–7a	6–7b	6–7c	6–8	168	44	49	32	50	169	182	214
SiO_2 (wt.%)	56.79	69.26	63.62	58.72	71.4	48.07	73.61	58.17	76.88	68.73	56.09	54.82	54.19	60.96	78.35
Al_2O_3	17.29	15.08	16.49	17.81	12.75	19.64	14.27	17.31	12	15	23.93	15.38	18.63	15.93	12.37
Fe_2O_3	11.31	5.7	8.2	7.55	5.6	12.79	2.55	11.09	3.15	5.49	7.19	13.15	10.35	8.78	1.56
MgO	5.35	1.95	3.25	2.94	2.5	10.29	1.77	4.85	1.17	2.87	5.21	4.93	5.53	4.35	0.57
CaO	1.74	1.77	3.54	6.82	0.87	4.05	0.87	0.55	2.54	1.56	1.24	7.08	4.15	3.64	1.8
Na_2O	5.63	4.91	2.31	2.23	5.69	3.95	4.17	6.31	1.43	4.83	0.74	3.15	5.55	4.43	4.27
K_2O	0.04	0.49	1.87	3.09	0.27	0.13	2.31	0.35	2.22	0.76	4.28	0.03	0.24	0.35	0.7
TiO_2	1.25	0.58	0.44	0.54	0.64	0.71	0.36	1.03	0.39	0.45	0.73	1.1	0.95	1.07	0.28
P_2O_5	0.29	0.17	0.13	0.1	0.18	0.13	0.07	0.17	0.1	0.11	0.06	0.14	0.16	0.25	0.05
MnO	0.31	0.08	0.11	0.21	0.13	0.28	0.05	0.13	0.05	0.12	0.06	0.19	0.2	0.18	0.01
Cr_2O_3	0.002	b.d.	b.d.	0.002	b.d.	0.004	b.d.	0.01	0.005	0.008	0.005	0.002	0.006	b.d.	0.003
LOI	4.4	2.2	5	5.5	2	5.4	2.8	3.2	2.4	2	4.8	3.7	4	3.3	1.4
Sum	99.88	99.9	99.83	99.77	99.91	99.86	99.85	99.89	99.89	99.92	99.8	99.8	99.81	99.85	99.93
Ba(ppm)	15	103	498	535	58	38	520	53	533	156	444	36	122	123	333
Ni	7.4	1.2	3.9	11.7	3.3	19.6	1.9	3.8	1.1	3.6	7.4	9.5	8.5	0.9	1
Sc	38	21	14	12	20	35	9	29	11	17	25	41	34	27	8
Co	22.1	5.3	7	7.3	7	30.8	2.7	23	3.6	8.6	9.6	35	22.2	14.1	1.1
Cs	b.d.	0.2	0.8	0.5	b.d.	b.d.	0.6	0.2	0.8	0.7	1	0.2	0.3	0.2	0.3
Hf	2	2.4	4.5	5.7	2.3	1.3	3.4	2.6	3.1	1.6	3.9	1.6	1.2	2.5	3.7
Nb	1.8	2.4	4.4	5	3.5	1.5	4.3	1.6	4.4	2.3	3.2	1.2	1.2	2.3	3.1
Rb	0.6	6.7	27.2	35.3	3.7	1.4	37.2	4.7	31	15.2	58	0.4	2.9	5.2	10
Sr	84.3	119.5	162.2	524.7	42.8	270	60.6	66.8	74.7	135.4	258	147.9	183.4	163.2	150.9
Ta	b.d.	0.1	0.3	0.4	0.2	b.d.	0.2	b.d.	0.2	b.d.	b.d.	b.d.	b.d.	b.d.	0.2
Th	0.6	0.7	3	7.2	2.3	2.9	5.8	1.1	2.9	1.5	3.6	0.2	0.4	0.8	2.1
U	0.1	0.2	0.7	0.8	0.6	0.7	1	0.4	1.1	0.1	b.d.	b.d.	b.d.	0.2	0.4
V	226	35	17	124	62	236	31	244	42	60	55	398	341	110	60
Zr	57.5	79.3	164.2	185.4	78.9	32.7	126	84.6	110.2	54.9	121.9	49.4	44.5	88.4	136
Y	36.3	29.9	28.8	26.9	29.3	15.4	22.4	20.8	28.8	17.1	23.2	24.5	20.8	36.3	41.1
La	5.5	7	11.8	23.5	13.8	8.9	18.1	6.7	12.4	7.9	7	5.1	5.6	9.5	12.1
Ce	10.6	15.9	27.4	40.7	29.8	17.3	41.2	19.6	23.5	14	17.3	10.4	12.3	20.6	25.9
Pr	2.19	2.55	3.59	5.4	3.9	2.15	4.04	2.1	3.17	1.84	2.39	1.76	1.89	3.15	3.68
Nd	11.6	13.1	16.6	20.4	17	9	17.7	10.5	13.2	9	11.6	9.3	9.4	15.4	17.4
Sm	3.42	3.64	4.02	4.43	4.25	2.13	3.42	3.2	3.35	2.39	3.48	2.71	2.24	4.35	4.4
Eu	1.38	1.28	1.08	1.23	1.05	0.79	0.92	0.8	0.81	1.01	0.95	1.04	0.96	1.48	1.14
Gd	5.13	5.36	4.49	4.61	4.78	2.51	3.81	3.42	4.27	2.72	4.05	3.69	3.43	5.6	5.89
Tb	0.91	0.88	0.83	0.82	0.82	0.46	0.65	0.65	0.8	0.54	0.78	0.68	0.61	1	1.06
Dy	5.69	5.86	5.07	4.92	4.97	2.91	3.53	3.86	4.95	3.15	4.74	4.45	4.06	6.01	6.65
Ho	1.26	1.08	0.99	1.06	1.14	0.62	0.8	0.7	1.07	0.67	1.14	0.89	0.77	1.3	1.43
Er	3.75	3.41	3.37	3.67	3.3	1.93	2.74	2.66	3.36	1.87	3.37	2.69	2.39	4.19	4.55
Tm	0.59	0.48	0.51	0.57	0.49	0.29	0.43	0.35	0.47	0.32	0.58	0.4	0.36	0.62	0.63
Yb	3.81	3.23	3.74	4.06	3.2	2	3.23	2.65	2.95	2.21	3.9	2.7	2.2	3.89	4.43
Lu	0.61	0.46	0.54	0.69	0.56	0.28	0.51	0.39	0.48	0.33	0.65	0.39	0.34	0.59	0.75

represented largely rhyodacitic/dacitic compositions. Type 2 rocks, however, were characterized by basaltic to basaltic-andesitic compositions (Figure 5). Both groups displayed enrichment in Th and La with respect to Nb when compared with normal mid-ocean ridge basalts (N-MORBs) (Th/Nb = 0.66–1.44 and La/Nb = 2.19–4.7 for Type 1; Th/Nb = 0.17–1.93 and La/Nb = 2.92–5.93 for Type 2; Th/Nb = 0.051 for N-MORBs; Sun and McDonough, 1989). Moreover, light REEs (LREEs) were variably enriched relative to heavy REEs (HREEs) in both types (Figure 6) ($[La/Yb]_N$ = 1.29–4.15 for Type 1; $[La/Yb]_N$ = 1.04–3.19 for Type 2). The enrichment was more prominent in the felsic members, which can be attributed to fractional crystallization, which lead to the enrichment of incompatible elements in the remaining liquid. Negative or positive Eu anomalies were present in some samples, which may suggest plagioclase fractionation or accumulation, respectively.

6.2. U-Pb zircon data

U-Pb zircon dating was performed on 3 metarhyolites of the KMs to reveal the crystallization age of the unit. The LA-ICP-MS U-Pb zircon dating results are presented in Table 2 and displayed in the diagrams of Figure 7. The zircons were colorless, with a long prismatic habit, mostly euhedral, and show oscillatory zoning (Figure 8).

A total of 5 zircon grains from Sample 24 had a $^{206}Pb/^{238}U$ lower intercept age of 113.2 ± 2.3 Ma (Table 2, Figure 7a). This age indicated radiogenic lead loss, but was within the error limits of zircons derived from Sample 184, as described below. From Sample 33, 7 zircon grains yielded a $^{206}Pb/^{238}U$ lower intercept age of 90 ± 52 Ma (Figure 7b). Because of the very high uncertainty in this sample, its age was not taken into consideration in the Discussion section. A total of 37 zircon grains from Sample 184 provided $^{206}Pb/^{238}U$ concordia ages between 91.8 and 105.1 Ma, with a weighted mean age of 94.64 ± 0.77 Ma (MSWD = 2.5) (Figures 7c and 7d).

The zircons from the metarhyolite samples yielded an early Late Cretaceous crystallization age for the protoliths of KMs. This finding was in accordance with the data of Aygül et al. (2015), which revealed the extrusion of the rocks as Late Cretaceous (93.8 ± 1.9 Ma and 94.4 ± 1.9 Ma) based on the U-Pb ages of only 6 zircon grains from 2 metarhyolite samples. Moreover, the Cenomanian-Turonian fossil findings from pelagic limestones in the equivalent of the Dikmen Formation (Yaylaçayı Volcanics of Tüysüz et al., 1995) constrained the upper age of volcanism.

Owing to the low-grade metamorphic conditions that the KMs had experienced, the zircon data did not

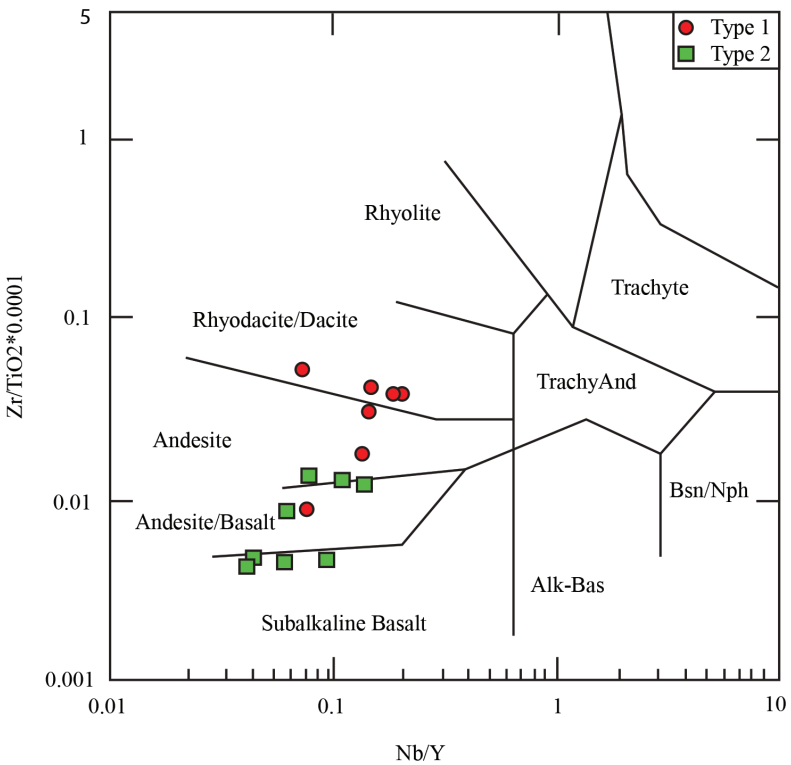

Figure 5. Chemical classification of the KMs on the basis of immobile elements (after Winchester and Floyd, 1977).

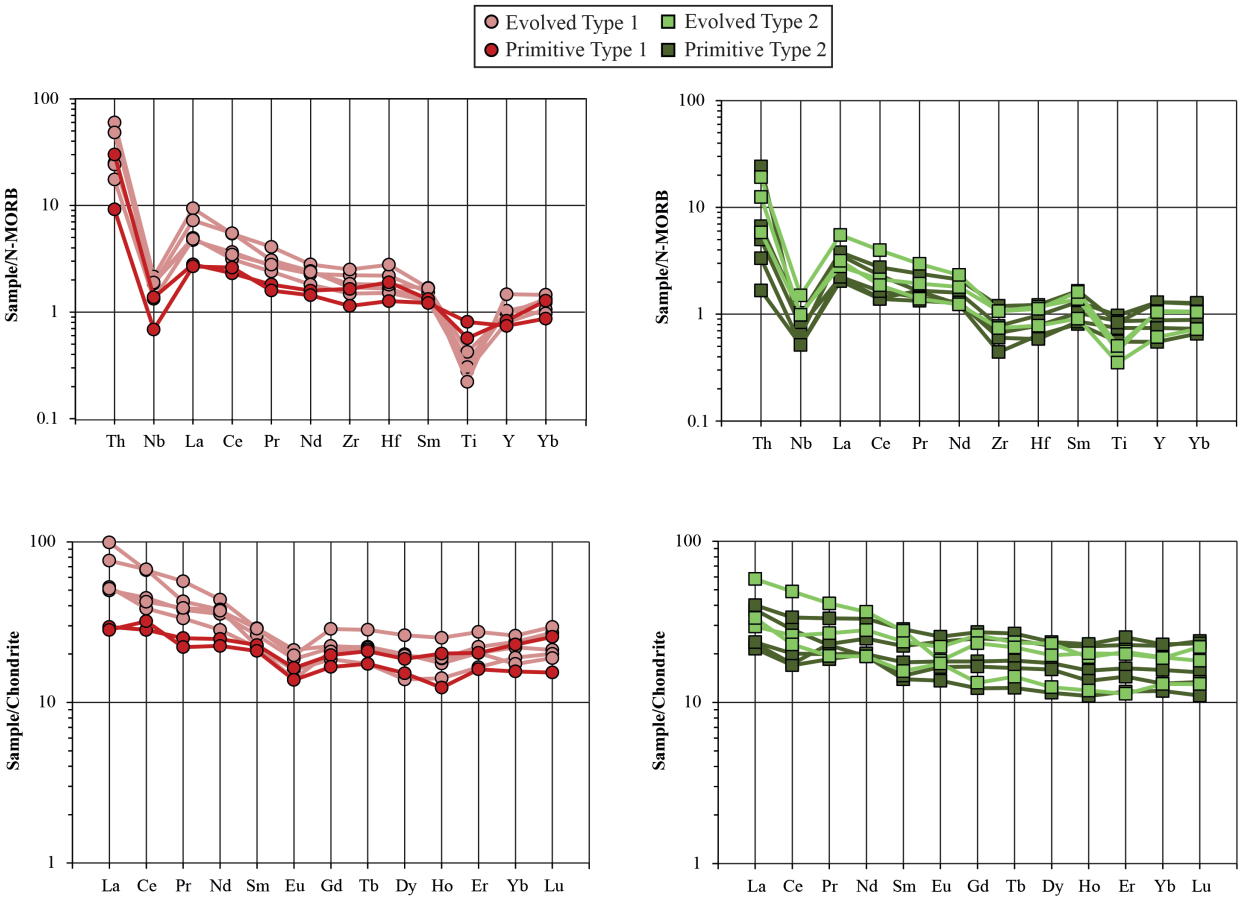

Figure 6. N-MORB normalized multielement and chondrite-normalized REE spidergrams of the KMs (normalization values for both the N-MORB and chondrite were taken from Sun and McDonough, 1989).

provide any information on the age of the metamorphism. However, Aygül et al. (2015) proposed a $^{40}Ar/^{39}Ar$ muscovite age of 69.9 ± 0.4 Ma (Danian-Maastrichtian) for the metamorphism of the KMs, which was in accordance with the available data.

7. Discussion

7.1. Assessment of the alterations

The investigated samples were affected by low-grade metamorphism, evidenced by loss on ignition values, ranging between 1.4 and 5.5 wt.%. Thus, all of the major oxide values were normalized to 100% on a volatile-free basis. Large ion lithophile elements (LILEs) (e.g., Sr, K, Rb, Ba) are known to be mobilized during low-grade metamorphism (e.g., Wood et al., 1976). In contrast, high field strength elements (HFSEs) (e.g., Ti, Zr, Y, Nb, Hf) and REEs behave relatively immobile during low-grade metamorphism (Pearce and Cann, 1973). To assess the elemental mobility of the KMs, a number of elements were plotted against Zr (a fluid-immobile element). The LILEs (e.g., K, Rb) displayed scattered distribution. On the other hand, the HFSEs and REEs (e.g., Yb, Nb, La, Eu) exhibited well-defined correlations, confirming their relatively immobile nature (Figure 9). Thus, the interpretations herein were mainly based on the immobile elements, as they are reliable indicators to infer the petrogenetic history.

7.2. Fractional crystallization

Both chemical groups of the KMs display a wide range of SiO_2 and MgO, which may suggest the control of fractional crystallization on the observed compositions. SiO_2 was chosen here as a differentiation index, which was plotted against several major and trace elements (Figure 10). Decreasing Fe_2O_3 and MgO contents, with increasing SiO_2 may indicate the fractionation of ferromagnesian minerals. The negative trends observed in the Ni, Co, and Cr were the another supporting evidence. Among these elements, Ni, and to a lesser extent, Co are known to be highly compatible with olivine (Kd_{Ni} and Kd_{Co} for olivine are 14 and 6.60, respectively; Rollinson, 1993). Thus, the negative trends of these elements against SiO_2 can be attributed to the fractionation of olivine. The negative correlation between Cr and SiO_2, however, can be related

Table 2. LA-ICP-MS U-Pb data for zircons in the Kösdağ Metarhyolites.

Sample number	Isotope ratios				Ages	
	207Pb/235U	2σ	206Pb/238U	2σ	206Pb/238Pb	2σ
Sample 24						
1	0.864	0.015	0.10354	0.00095	635.1	5.6
2	0.889	0.026	0.1117	0.0016	682.6	9.5
3	194	43	1.72	0.36	6140	880
4	0.1153	0.0055	0.01769	0.00035	113	2.2
5	61.4	3	0.554	0.037	2840	160
6	37.3	3.1	0.338	0.034	1860	160
7	11.21	0.4	0.1135	0.0044	692	25
Sample 33						
1	5.09	0.59	0.0526	0.0055	329	33
2	3.56	0.47	0.0477	0.0056	300	34
3	1.76	0.16	0.124	0.011	749	61
4	5.45	0.76	0.0586	0.0071	366	43
5	0.948	0.018	0.1129	0.0017	689	10
6	2.9	0.25	0.0362	0.003	229	19
7	0.877	0.02	0.1079	0.0016	660.2	9.3
Sample 184						
1	0.108	0.012	0.015	0.00053	95.9	3.4
2	0.1083	0.0098	0.01492	0.00048	95.4	3
3	0.148	0.014	0.015	0.00043	96	2.7
4	0.1081	0.0075	0.01522	0.00043	97.4	2.7
5	0.0972	0.0054	0.01463	0.00037	93.6	2.3
6	0.1039	0.0079	0.01469	0.00042	94	2.7
7	0.112	0.011	0.01644	0.00065	105.1	4.1
8	0.1041	0.0076	0.01445	0.00038	92.5	2.4
9	0.1055	0.006	0.01493	0.00043	95.5	2.7
10	0.1037	0.0053	0.01518	0.00036	97.1	2.3
11	0.113	0.015	0.01493	0.0006	95.5	3.8
12	0.0975	0.0077	0.01499	0.00047	95.9	3
13	0.1039	0.0091	0.01519	0.00046	97.2	2.9
14	0.1071	0.0074	0.01434	0.00062	91.8	3.9
15	0.104	0.011	0.01456	0.00058	93.2	3.7
16	0.107	0.011	0.01476	0.00049	94.4	3.1
17	0.129	0.011	0.01535	0.00047	98.2	3
18	0.1002	0.0089	0.01467	0.00049	93.9	3.1
19	0.12	0.011	0.0163	0.00059	104.2	3.8
20	0.1042	0.0056	0.01484	0.0004	95.3	2.6
21	0.1025	0.0046	0.01455	0.00032	93.1	2.1
22	0.098	0.0069	0.01437	0.00035	91.9	2.2
23	0.0977	0.0031	0.01469	0.00033	94	2.1

Table 2. (Continued).

24	0.1032	0.0092	0.01476	0.00048	94.5	3
25	0.09	0.011	0.01518	0.00055	97.1	3.5
26	0.124	0.011	0.01531	0.00041	97.9	2.6
27	0.0869	0.0094	0.01435	0.00039	91.9	2.5
28	0.0992	0.0064	0.01437	0.00042	92	2.7
29	0.1152	0.0059	0.0162	0.0006	103.6	3.8
30	0.0803	0.0082	0.01434	0.00051	91.8	3.2
31	0.0972	0.0054	0.0143	0.00046	91.5	2.9
32	0.099	0.012	0.01502	0.00069	96.1	4.4
33	0.109	0.011	0.0144	0.00043	92.1	2.7
34	0.125	0.012	0.01497	0.00064	95.8	4.1
35	0.0948	0.0033	0.01469	0.00034	94	2.1
36	0.1273	0.0068	0.01561	0.00041	99.8	2.6
37	0.1017	0.0094	0.01505	0.0005	96.3	3.2

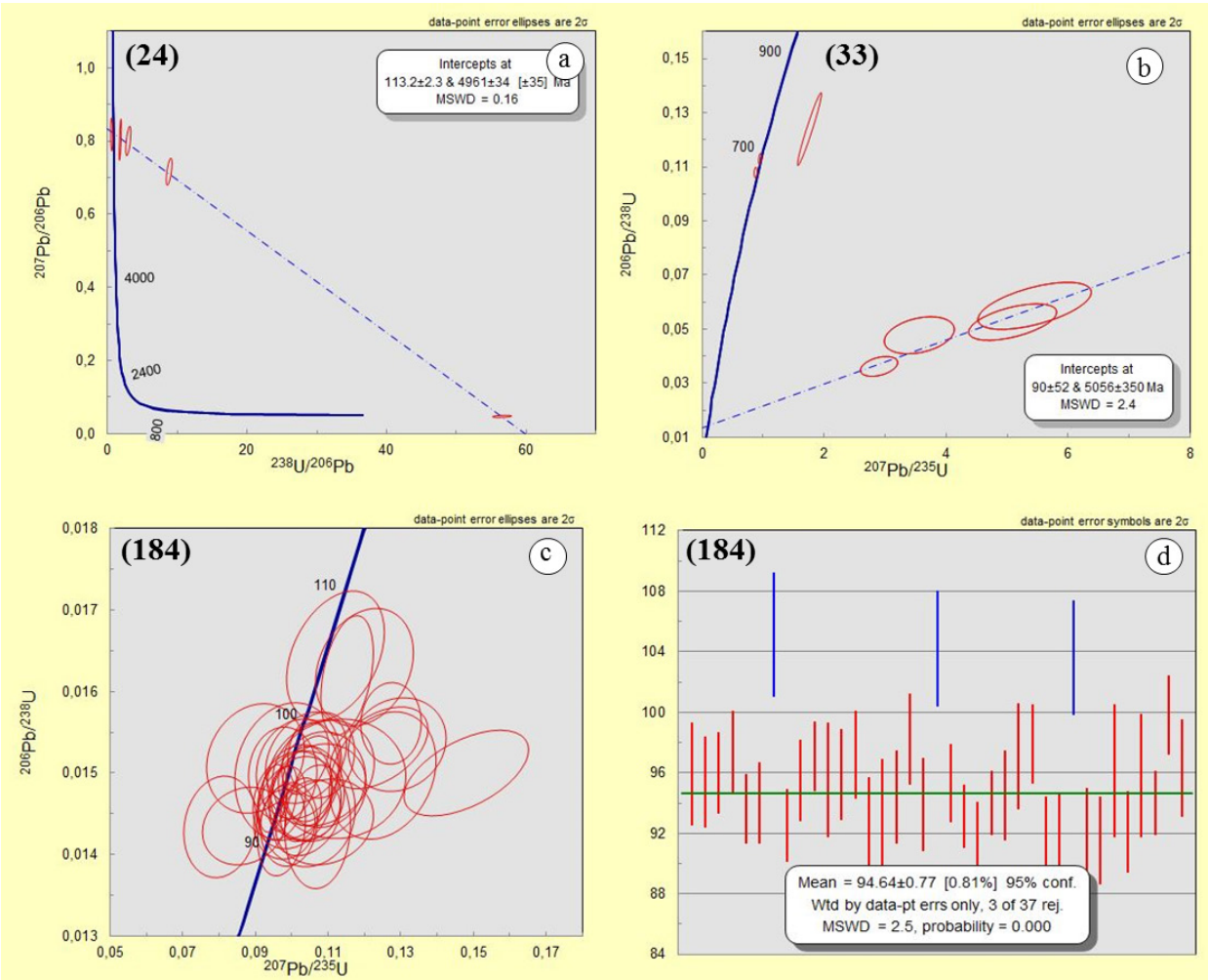

Figure 7. $^{206}Pb/^{238}U$ vs $^{207}Pb/^{235}U$ diagrams for samples 24, 33, and 184 of the KMs. (a) Lower intercept age for sample 24. (b) Lower intercept age for sample 33. (c) Concordia age for sample 184. (d) Weighted mean age values for sample 184.

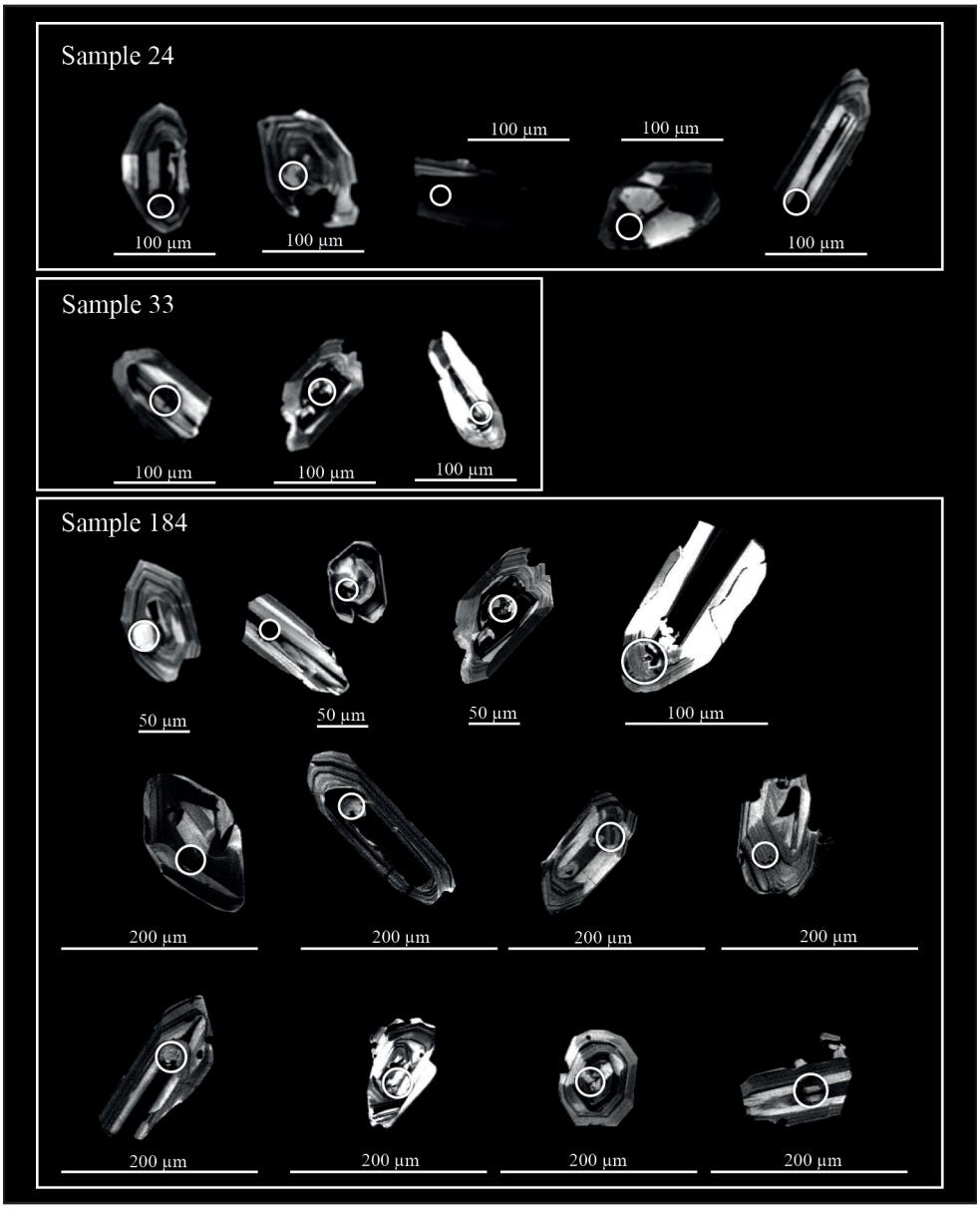

Figure 8. Cathodoluminescence images of typical zircons from metarhyolite samples 24, 33, and 184.

to pyroxene fractionation (particularly clinopyroxene; Kd_{Cr} = 34 for clinopyroxene; Rollinson, 1993). In both groups, decreasing Al_2O_3 contents against increasing SiO_2 indicated plagioclase fractionation. The negative correlations of Y, Zr and TiO_2 with SiO_2 (observed for SiO_2 ≥ ~60 wt.%), on the other hand, can be explained by the fractionation of Fe-Ti oxides.

In summary, olivine, pyroxene, plagioclase, and Fe-Ti oxides can be regarded as critical fractionating phases, which potentially modified the composition of the magma during the postmelting stage of the KMs. It must also be noted that two chemical groups displayed somewhat overlapping SiO_2 (and MgO) compositions and the Type 1 samples displayed higher Zr and Hf abundances for a given SiO_2 content. This suggested that two groups were not related to each other via fractional crystallization processes; thus, the diverse chemical signatures appeared to be an artifact of the mantle source and/or partial melting.

7.3. Mantle source characteristics

The KMs displayed an extensive range of chemical composition, spanning from basalt to dacite. It must be noted, however, that only the primitive samples (MgO >4.00 wt.%) in the dataset were taken into consideration in order to minimize the effects of fractional crystallization,

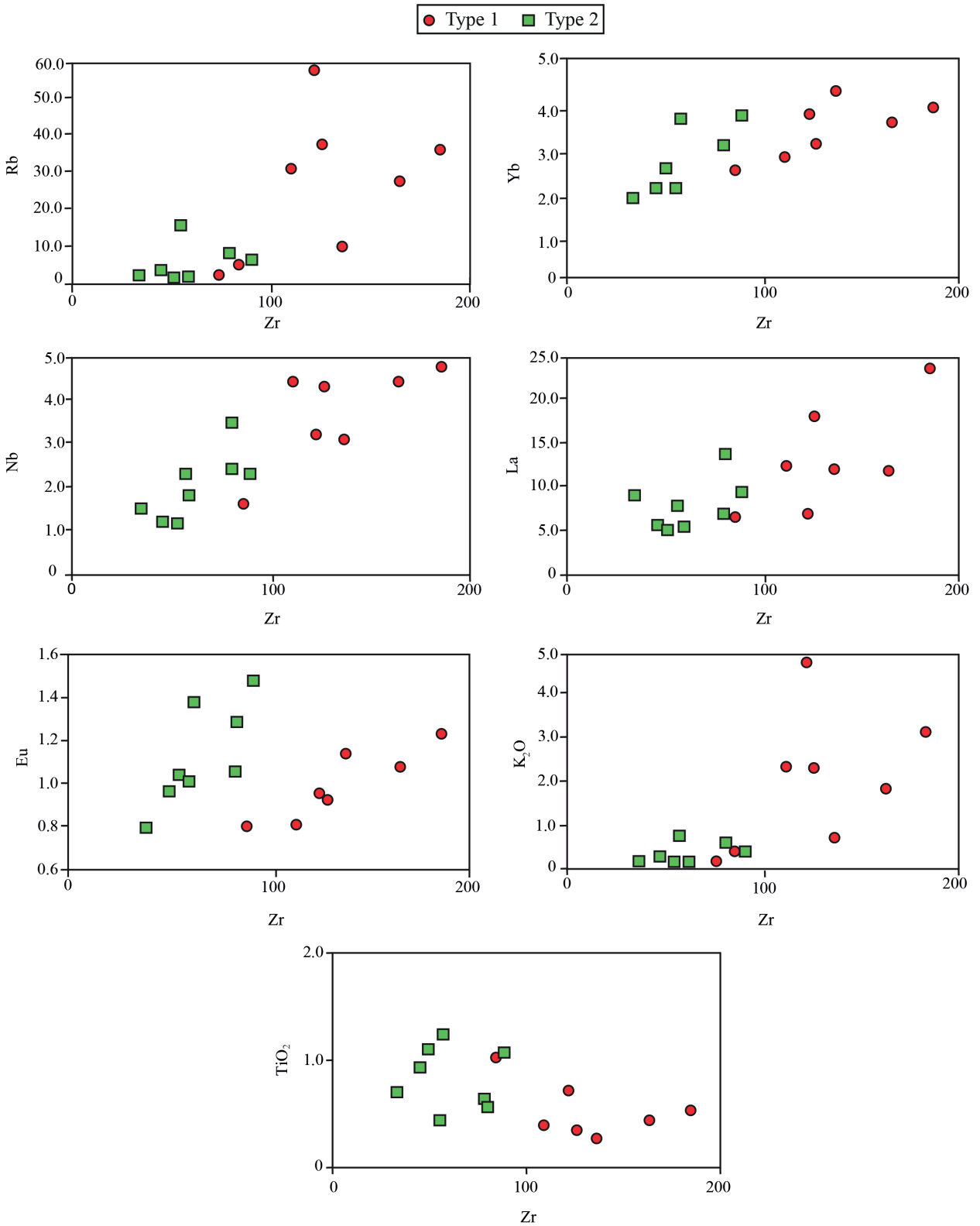

Figure 9. Plots of the selected major oxides and trace elements against Zr to assess mobility.

which in turn would allow a more reliable interpretation about the source characteristics to be conducted. When the compatibilities of the trace elements were considered during partial melting of lherzolite under upper mantle conditions, Nb is known to be more incompatible relative to Zr (e.g., Sun and McDonough, 1989). Consequently, Nb

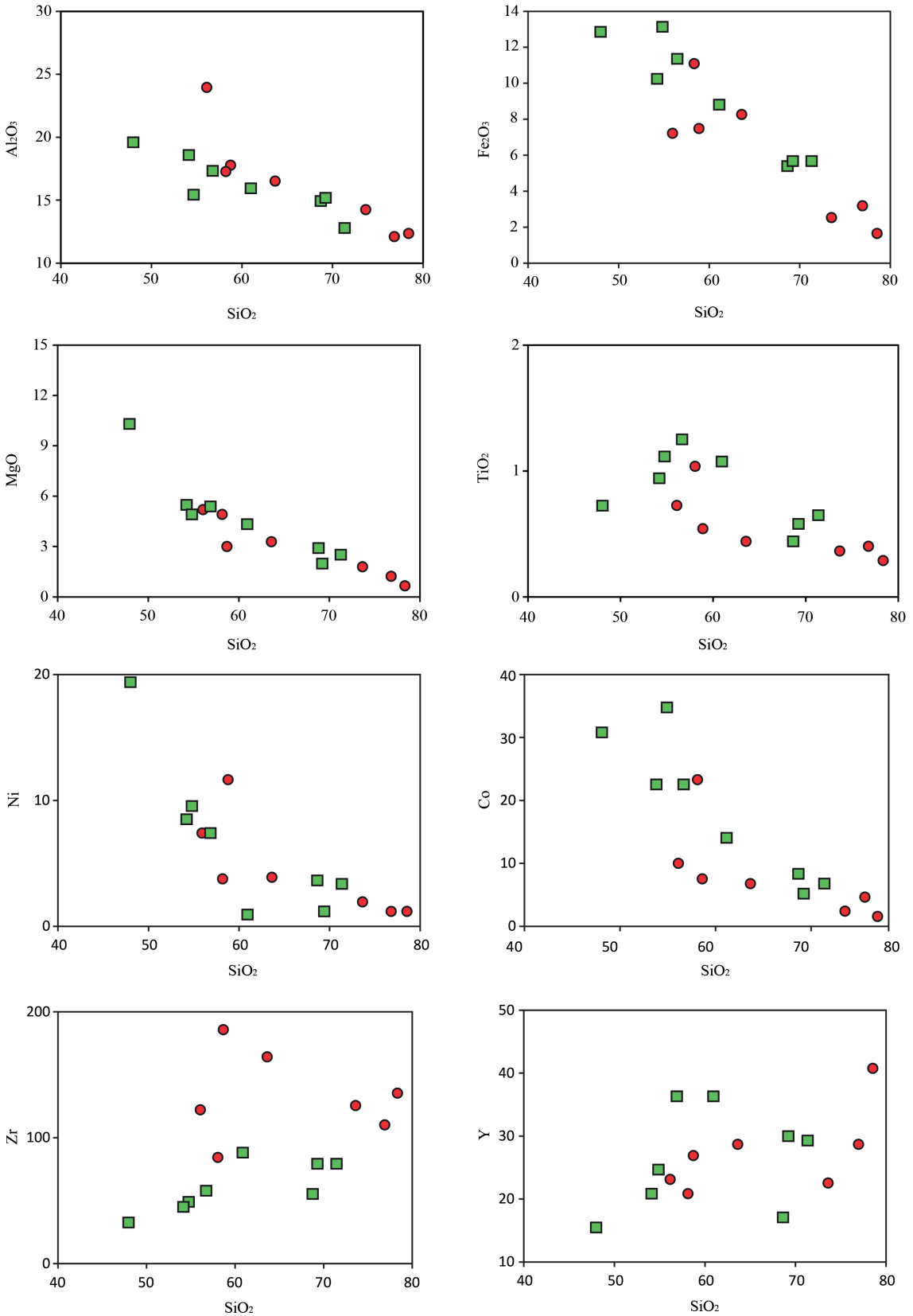

Figure 10. Harker variation diagrams for the Kösdağ metavolcanic rocks (the symbols are the same as in Figure 9).

tends to be removed from the source region during melt extraction, which in turn would increase the Zr/Nb ratio of the source. Therefore, high Zr/Nb ratios may indicate the involvement of depleted sources, as was the case for the N-MORBs (Zr/Nb = 31.8; Sun and McDonough, 1989). In contrast, lower Zr/Nb ratios may suggest a contribution from enriched mantle sources and/or low degrees of melting, such as ocean island basalts (OIBs) (Zr/Nb = 5.83 Sun and McDonough, 1989). The Zr/Nb ratio of the Type 1 samples ranged between 38.1 and 52.9 (average = 45.5), while this ratio spanned from 21.8 to 41.2 (average = 34.1) in the Type 2 samples. These values were somewhat similar to the Zr/Nb ratio of the N-MORBs (N-MORB Zr/Nb = 31.86; Sun and McDonough, 1989) that have been generated mainly from depleted mantle sources (Figure 11a). Thus, the KMs appeared to have primarily involved depleted sources in their petrogenesis.

Another parameter that may help to track the nature of the source is the Zr/Y ratio. In this pair, Zr is more incompatible than Y; thus, while melts characterized by high Zr/Y ratios may indicate strong contribution from enriched mantle sources (also associated with low degrees of melting), such as that of OIBs (OIB Zr/Y = 9.66; Sun and McDonough, 1989), low Zr/Y ratios may imply an origin largely involving depleted mantle sources, such as N-MORBs (N-MORB Zr/Y = 2.64; Sun and McDonough, 1989) (Figure 11b). In the KMs, the Zr/Y ratios of the Type 1 samples ranged between 4.07 and 5.25, while those of the Type 2 samples ranged from 1.58 to 2.44.

Therefore, on the basis of the Zr/Y ratio, it can be suggested that most of the samples were dominantly derived from depleted mantle sources. It must be noted, however, that the Type 1 samples may have also included some contribution from enriched mantle sources, owing to their higher Zr/Y ratios. The Nb/Y ratios can also be used in a way similar to the Zr/Y ratios, such that melts with low Nb/Y ratios are associated with depleted mantle sources, whereas high Nb/Y ratios may be suggestive of enriched sources (N-MORB Nb/Y = 0.08, OIB Nb/Y = 1.65; Sun and McDonough, 1989) (Figure 11b). The Nb/Y ratios for the Type 1 samples ranged between 0.08 and 0.14, while the Type 2 samples ranged between 0.05 and 0.10. This supported the idea that the KMs have acquired a dominant contribution of the depleted sources.

Depletion in Nb (and Ta) relative to Th and La is a characteristic property of subduction zone magmas, attributed to fluid/melt transport in the shallow parts of subduction zones (e.g., Pearce and Peate, 1995). This feature was also observed in the KMs, which reflected strong Nb depletion when compared to Th and La (Figure 6). In contrast to Nb, which is strongly retained in slab (due to its compatibility with rutile, e.g., Ayers and Watson, 1993), La (and other LREE) and Th are both mobilized by slab-derived melt. They are efficiently removed from the slab during subduction, and therefore, the overlying mantle wedge becomes enriched in Th and La relative to Nb. Thus, high Th/Nb and La/Nb ratios are the characteristic features of magmas generated above subduction zones (Average Mariana Arc Th/Nb = 0.25, La/Nb = ~2.50, Pearce et al., 2005). While the La/Nb ratio of the Type 1 samples ranged between 2.19 and 4.19, that of the Type 2 samples ranged from 3.06 to 5.93 (Figure 11c). Such high values may suggest a subduction-modified mantle source for the KMs.

This idea can be further tested using a Th/Yb-Nb/Yb plot, which is very useful to trace subduction-related processes, as well as source characteristics (Pearce and Peate, 1995) (Figure 11d). Trace elements Nb and Th exhibit similar geochemical behavior during the melting of upper mantle peridotite (e.g., Sun and McDonough, 1989). However, during slab melting, the behaviors of these two2 elements become decoupled; while Nb is subduction-immobile and retained in the slab, Th is subduction-mobile and transferred via slab-melts into the mantle wedge. Thus, on the Th/Yb-Nb/Yb plot, the nonsubduction-related melts (MORBs and OIBs) will define an array, while the subduction-related melt compositions will be displaced above the array due to relative enrichment in Th in their mantle sources. On this plot, all of the KM samples appeared to plot above the array, implying the effect of the subduction component. Moreover, crustal contamination may have had a similar effect due to the composition of continental crust, which will be discussed below (Figure 11d).

In the same plot, the Nb/Yb ratios of the KMs were mostly lower than that of the average N-MORB (N-MORB Nb/Yb = 0.76; Sun and McDonough, 1989). The Nb/Yb ratio acts very similar to the Nb/Y ratio, since Nb is more incompatible than Yb. Thus, low Nb/Yb ratios are characteristic features of depleted mantle sources. Therefore, this result also strengthened the idea of the predominant involvement of depleted sources in the petrogenesis of the KMs. It must also be noted that the lower Nb/Yb values characteristic of Type 2, in general, relative to Type 1, may indicate the more depleted nature of the former, which was probably linked to previous melt extraction (Figure 11d).

The Th(La)-Nb-Yb systematics strongly implied that the KMs comprised slab-derived contributions in their mantle sources (Figures 11c and 11d). In this regard, the relative enrichment in Th and La may suggest their mobilization via sediment melt (e.g., Elliott et al., 1997), since these elements are not readily transported by aqueous fluids (e.g., Pearce and Peate, 1995). Partial melting of the slab tends to preferentially enrich Th and La over Nb in the melt (provided that a titanate residual phase is present, like

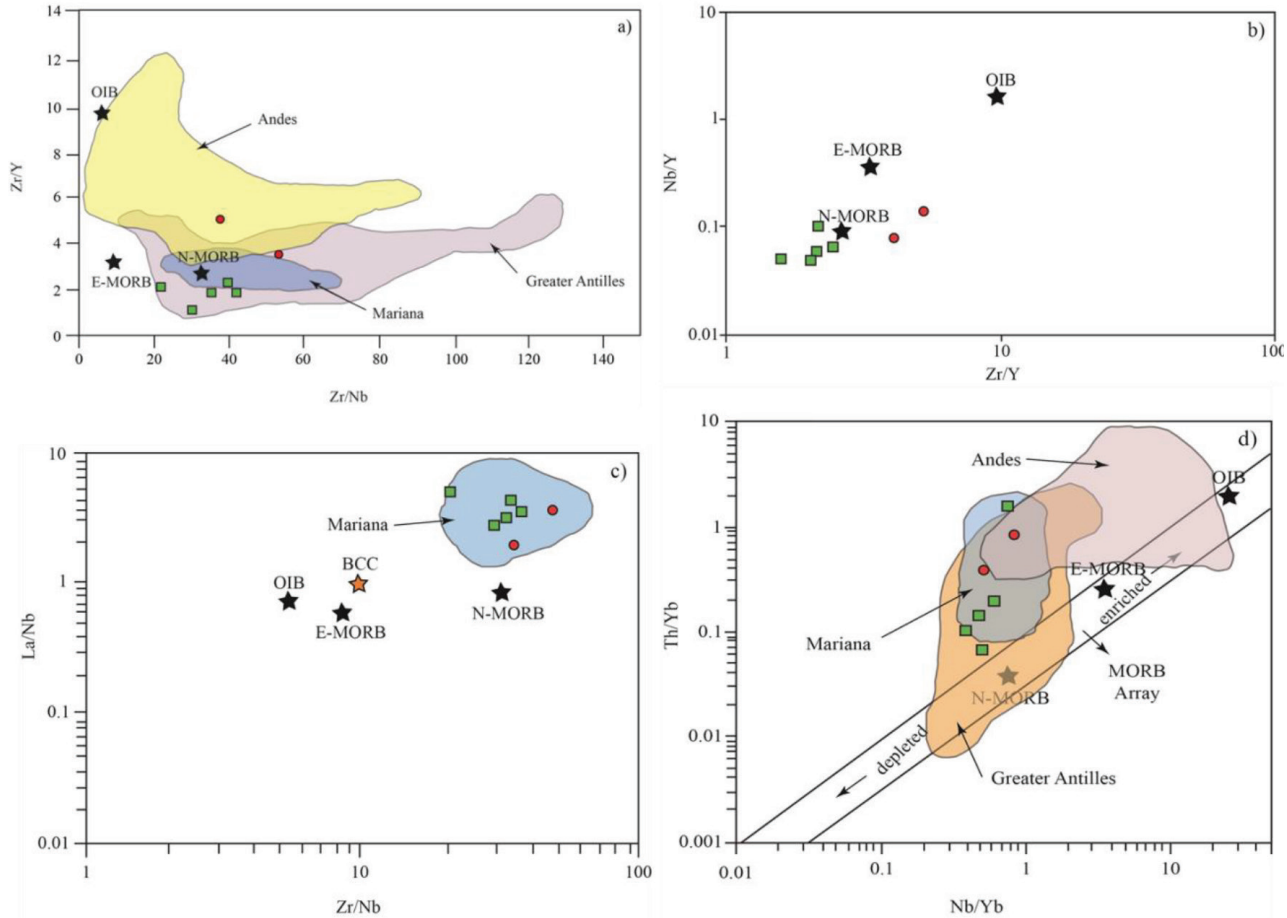

Figure 11. a) Zr/Nb vs. Zr/Y diagram. Greater Antilles data were taken from Jolly et al. (1998) and Jolly (2001); Andes data were taken from a compilation by Winter (2001); and Mariana data were taken from Pearce et al. (2005). b) Zr/Y vs. Nb/Y diagram (the average N-MORB, enriched mid-ocean ridge basalt (E-MORB), and OIB values were taken from Sun and McDonough, 1989). c) Zr/Nb vs. La/Nb diagram (N-MORBs, E-MORBs, and OIB values were taken from Sun and McDonough (1989). BCC values were taken from Taylor and McLennan (1995). d) Variation of Nb/Yb against Th/Yb on the KMs (after Pearce and Peate, 1995). Average N-MORB, E-MORB, and OIB values were taken from Sun and McDonough (1989). Greater Antilles data were taken from Jolly et al. (1998); Jolly (2001); the Andes data were taken from a compilation by Winter (2001), Mariana data were taken from Pearce et al. (2005).

rutile). It must be noted, however, that the nature of the slab melt is also controlled by the chemical composition of the subducted sediments. Sediments are typically enriched in Th and La (over Nb), although they display variable enrichment/depletion in Zr-Hf (e.g., Plank and Langmuir, 1998). Consequently, it was expected that these geochemical features would be imprinted on the subduction-related magmas with the variable addition of the subduction component. Considering the bulk composition of sediment columns subducted at trenches, the Izu-Bonin sediment, for example, is Zr-Hf depleted, whereas for the South Sandwich sediment, this depletion does not exist. Therefore, although the subduction component is a common feature for both groups of the KMs, the composition (and possibly the mass fraction) of sediment that has been involved in their mantle sources appeared to be different.

Another issue to consider was that high La/Nb and Th/Nb ratios may also indicate the influence of crustal contamination. Bulk continental crust (BCC) is represented by relatively high La/Nb and Th/Nb ratios (1.45 and 0.32, respectively) (Taylor and McLennan, 1995). However, the KMs showed much higher values of La/Nb and Th/Nb relative to the BCC, suggesting that these ratios were predominantly controlled by the subduction component rather than crustal contamination. This issue, however, cannot be entirely excluded at this point.

7.4. Tectonomagmatic constraints

The KM samples showed spiked trace element patterns in the N-MORB normalized spidergrams (Figure 6). Selective enrichment in Th and LREE over HFSE suggested that the mantle source has been modified by a subduction component (i.e. fluids, melts) derived from the subducted

slab (e.g., Pearce and Peate, 1995). Such features are not observed in the oceanic magmas generated away from subduction zones (i.e. N-MORBs and OIBs).

As shown by the discrimination diagrams (Figures 12a and 12b), the trace element systematics of the KMs were in line with an origin from a subduction zone. A further question to answer is whether these arc-related volcanics are of oceanic or continental origin. Magmas of the oceanic arcs are typically characterized by low Nb/Yb ratios (Average Greater Antilles Nb/Yb = 0.68: Jolly et al., 1998; Jolly, 2001; Average Mariana Nb/Yb = 1.22; Pearce et al., 2005) (Figure 11d), whereas magmas of the continental arcs exhibit higher values (Average Andes Nb/Yb = 3.22; Winter, 2001). The volcanic protoliths of the KMs had low Nb/Yb ratios (an average of 0.47), thus implying oceanic arc affinities. This result was also confirmed by high Zr/Nb ratios; the high values of Zr/Nb were indicative of an oceanic origin, whereas low values would imply arcs of continental character (Average Greater Antilles Zr/Nb = 52.89; Jolly et al., 1998; Jolly, 2001; Average Mariana = 39.13; Pearce et al., 2005; Average Andes Zr/Nb = 30.8; Winter, 2001) (Figure 11a).

The average Zr/Nb ratio of the samples was 37.34, therefore suggesting that an oceanic arc origin was more likely than a continental arc for the KMs. The trace element systematics, which are characterized by relative enrichment in subduction-mobile Th and La coupled with N-MORB-like HFSE abundances, also indicated that the KMs were produced above an intraoceanic subduction zone (Figure 13). The idea of an oceanic arc was also in accordance with the previous studies on the KM rocks, as well as their equivalents in northern Turkey (Tüysüz, 1990; Tüysüz et al., 1995; Berber et al., 2014; Aygül et al., 2015). In detail, the geochemical characteristics of the KMs are consistent with those of the Late Cretaceous Yaylaçayı Volcanics of Tüysüz et al. (1995) and Kösdağ Formation of Aygül et al. (2015) (Figure 13). Both the rocks of the KMs and volcanics of the Kösdağ Formation showed relative enrichment in LREEs with respect to HREEs. Although the volcanic rocks of the Yaylaçayı unit were not evaluated on the chondrite-normalized REE spidergrams, due to the lack of REE data by Tüysüz et al. (1995), their tectonomagmatic features inferred from other trace elements were very similar. This similarity indicated a genetic relationship between the different tectonic units of the IAESB.

7.5. Geodynamic implications

Regarding the overall evolution of the IAESB, there is a consensus that its mélange complexes were generated during the Late Cretaceous closure of the IAE Ocean (IAEO), which is the main Neotethyan oceanic seaway in Turkey (for details, please see Göncüoğlu et al., 2010). The mélange complexes comprise several slide-blocks with radiolarian cherts and/or pelagic carbonates in depositional association with pillow lavas. The radiolarian ages obtained from these oceanic sediments indicated that the oceanic crust generation within the IAEO continued from the Triassic to the end of the Early Cretaceous (e.g., Bortolotti et al., 2013; 2018; Göncüoğlu et al., 2015), and produced ridge-, as well as suprasubduction-type, ophiolitic rocks on its different segments.

The formation of the suprasubduction-type ophiolites (including oceanic arcs), as well as the formation of subophiolitic metamorphic soles, are overall pieces of evidence for the onset of intraoceanic subduction within the İAEO (e.g., Floyd et al., 2000; Çelik et al., 2011; Parlak et al., 2012). This intraoceanic subduction likely started in the Jurassic period in the IAEO (e.g., Göncüoğlu et al., 2010) and continued to as late as the mid-Late Cretaceous (Turonian—Yalınız et al., 1996; Barremian-Aptian—Bortolotti et al., 2013; Özkan et al., 2020), probably in different segments, leading to the production of suprasubduction zone (SSZ)-type rocks.

The presence of ensimatic arcs within the IAEO was already suggested on the basis of geochemical data from the Central Anatolian Ophiolites (Göncüoğlu et al., 1991; Yalınız et al., 1996) in the Central Anatolian Crystalline Complex, and from the Yaylaçayı Volcanics (Tüysüz et al., 1995) to the NE of Yapraklı in the southern Central Pontides (Figure 1b). The oceanic arc-type characteristics, such as low Nb concentrations coupled with relative enrichment in subduction-mobile elements Th and La), have been exemplified (Figures 6, 11, and 13) by the new geochemical data herein. In addition, the new zircon U-Pb ages (Figures 7 and 8) obtained from the Kösdağ volcanic rocks indicated the formation of early Late Cretaceous (Cenomanian) oceanic arc-type magmatic events.

In the current model (Figure 14), it was proposed that theIAEO between the Tauride-Anatolide/Central Anatolian Units and the SCT was already narrowing during the mid-Cretaceous by multiple subduction zones. Of these, the northern one beneath the SCT produced the Tafano continental arc (Ellero et al., 2015b) in the southern Central Pontides during the Late Cretaceous. The other subduction, an intraoceanic one that produced the Kösdağ island arc type volcanics (and the Yaylaçayı Volcanics of Tüysüz et al., 1995), probably started during the early Late Cretaceous. This intraoceanic subduction was initially interpreted as northward-directed by Yalınız et al. (1996), whereas Tüysüz et al. (1995) proposed an intraoceanic subduction model with alternative subductions to the north as well as to the south. Further, huge slide blocks, which were representatives of this arc, together with remnants of fore-and back-arc (SSZ)-type oceanic lithosphere, are now found within the Ankara Mélange and in its eastward and westward continuations (e.g., Göncüoğlu et al., 2010;

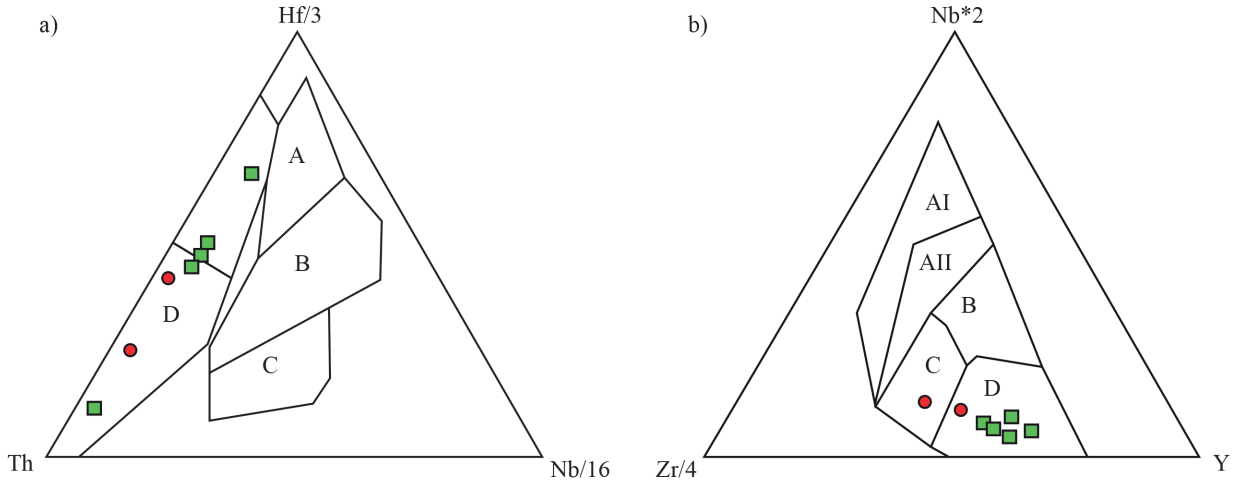

Figure 12. Tectonic discrimination diagrams for the KMs. a) After Wood et al. (1979). Fields: A: N-MORB; B: plume-ridge-MORBs; C: WPD (writhin plate basalts; and D: destructive plate margin basalts. b) After Meschede (1986). Fields; AI and AII: WPB; B: PMORB; C: WPT (written plate tholeiites), and VAB; D: N-MORB and VAB.

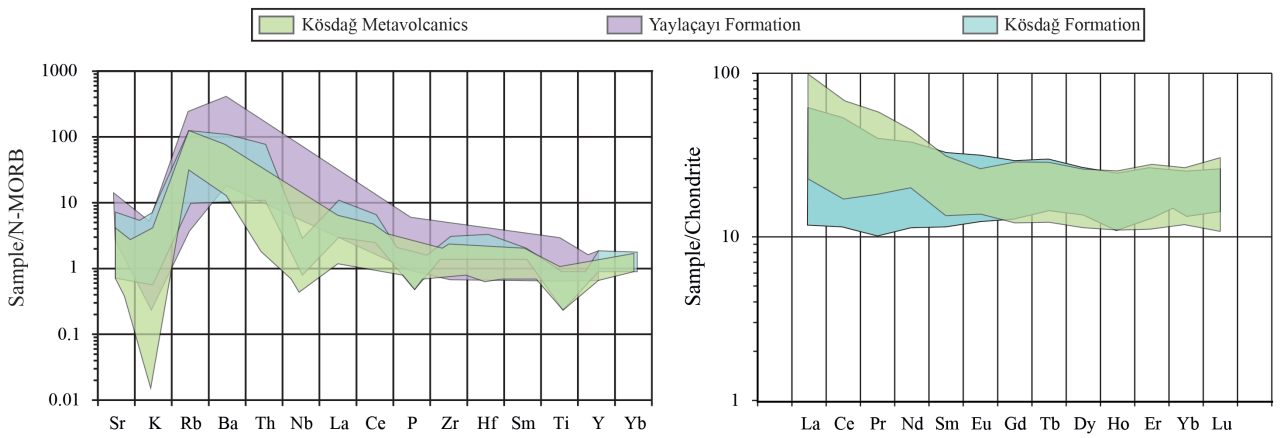

Figure 13. N-MORB-normalized multielement and chondrite-normalized REE spidergrams of the KMs, Yaylaçayı Formation, and Kösdağ Formation (normalization values for both the N-MORB and chondrite data were taken from Sun and McDonough (1989). Yaylaçayı Formation data were taken from Tüysüz et al. (1995) and Kösdağ Formation data were taken from Aygül et al. (2015).

2015; Dangerfield et al., 2011; Bortolotti et al., 2013; 2018). This arc and pieces of the SSZ-type oceanic lithosphere were thrusted onto the northern margin of the Central Anatolian Crystalline Complex (e.g., Yalınız et al., 1996). The final closure of the IAEO in the southern Central Pontides should have occurred later in the Early Eocene, as evidenced by the earliest common Middle Eocene overstep sequence covering the main alpine tectonic units (Ottria et al., 2017).

8. Conclusions

The KMs in the southern Central Pontides are represented by metavolcanic rocks, consisting of metadacites, metaandesites, and metabasalts, that have been affected by low-grade metamorphism and subsequent deformations. The studied rocks are interbedded with recrystallized pelagic limestone, chert, and mudstone, and unconformably overlain by Campanian-Maastrichtian limestones. The geochemistry of the metavolcanic rocks indicated an intraoceanic subduction volcanism, evidenced by the low abundances and depleted nature of HFSEs (Ti and Nb) and enrichment in subduction-mobile elements (particularly Th and La). On the basis of their relative Zr-Hf enrichment/depletion, the rocks of the KMs were subdivided into two chemical types, as Type 1 and Type 2. Both types geochemically correlated to the Mariana arc in the western Pacific Ocean. The high Zr/Nb, low Zr/Y, and Nb/Y signatures of the KM rocks indicated that they were derived from a depleted source similar to a N-MORB source, modified by a subduction component.

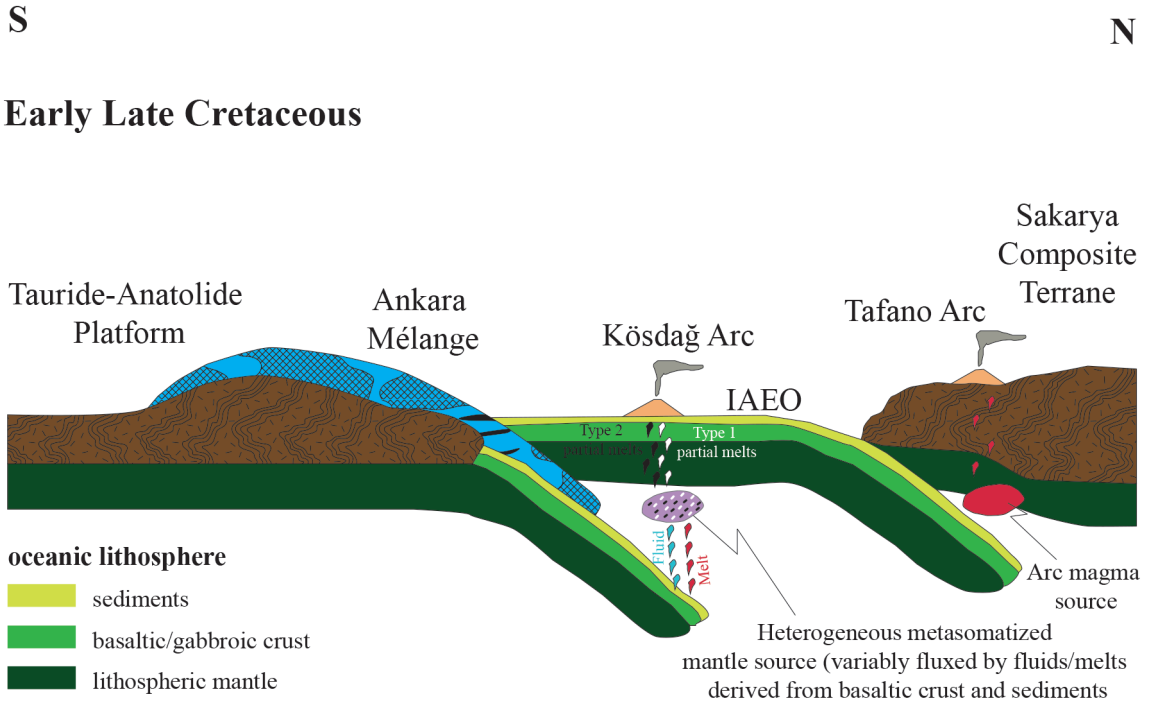

Figure 14. Suggested geodynamic and petrogenetic model for the tectonomagmatic evolution of the KMs (for details see the Discussion section).

Zircons from the metarhyolite samples yielded LA-ICP-MS U-Pb ages ranging between 113.2 ± 2.3 and 94.64 ± 0.77 Ma, indicating that the volcanic precursors of the KMs were formed during the early Late Cretaceous.

Considering the overall regional geodynamic evolution of the northern branch of the Neotethys, this new data confirmed that the KMs were formed as part of a larger island arc above an intra oceanic subduction within the IAEO during the early Late Cretaceous.

Acknowledgments

The authors gratefully thank Quentin Crowley from the Department of Geology of Trinity College in Dublin for the U-Pb analyses, as well as Alican Aktağ and Okay Çimen for their assistance during field work. The constructive comments of three anonymous referees are gratefully acknowledged. This research was supported by the ÖYP (Faculty Development Program) project from METU and a METU Scientific Research Projects (BAP) grant (BAP-03-09-2015-002).

References

Ayers JC, Watson EB (1993). Rutile solubility and mobility in supercritical aqueous fluids. Contributions to Mineralogy and Petrology 114: 321-330.

Aygül M, Okay AI, Oberhansli R, Schmidt A, Sudo M (2015). Late Cretaceous infant intra-oceanic arc volcanism, the Central Pontides, Turkey: Petrogenetic and tectonic implications. Journal of Asian Earth Sciences 111: 312-327.

Berber F, Göncüoğlu MC, Sayıt K (2014). Geochemistry and tectonic significance of the Kösedağ Metavolcanic rocks from the Sakarya Zone, Northern Turkey. In: Proceedings of 20th CBGA Congress; Tirana, Albania. Abstract Book 1: pp. 161-163.

Bortolotti V, Chiari M, Göncüoğlu MC, Marcucci M, Principi G et al. (2013). Age and geochemistry of basalt-chert associations in the ophiolites of the Izmir-Ankara Mélange, east of Ankara, Turkey: Preliminary data. Ofioliti 38: 157-173.

Bortolotti V, Chiari M, Göncüoğlu MC, Principi G, Saccani E et al. (2018). The Jurassic-Early Cretaceous basalt-chert association in the ophiolites of the Ankara Mélange east of Ankara, Turkey: age and geochemistry. Geological Magazine 155: 451-478.

Çakıroglu, R.E., Göncüoğlu, MC, Marroni, M.&Pandolfi, L. (2013). Andesitic dyke swarms in the Araç-Boyalı foredeep basin, N Anatolia: Evidence for Eocene extension. Mineralogical Magazine 77: 808.

Catanzariti R, Ellero A, Göncüoğlu MC, Marroni M, Ottria G et al. (2013). The Taraklı Flysch in the Boyali area (Sakarya Terrane, northern Turkey): Implications for the tetonic history of the Intra Pontide suture zone. Comptes Rendus Geoscience 345: 454-461.

Çelik ÖF, Marzoli A, Marschik R, Chiaradia M, Neubauer F et al. (2011). Early-Middle Jurassic intra-oceanic subduction in the İzmir-Ankara-Erzincan Ocean, Northern Turkey. Tectonophysics 509: 120-134.

Dangerfield A, Harris R, Sarıfakıoğlu E, Dilek Y (2011). Tectonic evolution of the Ankara Mélange and associated Eldivan ophiolite near Hançili, central Turkey. The Geological Society of America Special Paper 480: 143-169.

Ellero A, Ottria G, Marroni M, Pandolfi L, Göncüoğlu MC (2015a). Analysis of the North Anatolian Shear Zone in Central Pontides (northern Turkey): Insight for geometries and kinematics of deformation structures in a transpressional zone. Journal of Structural Geology 72: 124-141.

Ellero A, Ottria G, Sayit K, Catanzariti R, Frassi C et al. (2015b). Geological and geochemical evidence for a Late Cretaceous continental arc in the central Pontides, northern Turkey. Ofioliti, 40 (2), 73-90.

Floyd PA, Göncüoğlu MC, Winchester JA, Yalınız MK (2000). Geochemical character and tectonic environment of Neotethyan ophiolitic fragments and metabasites in the Central Anatolian Crystalline Complex, Turkey. In: Tectonics and Magmatism in Turkey and its surroundings, In: Bozkurt E, Winchester JA, Piper J (editors), Geological Society of London Special Publication 173: 183-202.

Frassi C, Göncüoğlu MC, Marroni M, Pandolfi L, Ruffini et al. (2016). The Intra-Pontide suture zone in the Tosya-Kastamonu area, Northern Turkey. Journal of Maps 12: 211-219.

Okay AI, Tüysüz O, Satır M, Altıner SÖ, Sherlock S et al. (2006). Cretaceous and Triassic subduction-accretion, high pressure-low temperature metamorphism, and continental growth in the Central Pontides, Turkey. Geological Society of America Bulletin, 118, 1247-1269.

Göncüoglu MC (2010). Introduction to the Geology of Turkey: Geodynamic evolution of the pre-Alpine and Alpine terranes. Ankara, Turkey: MTA.

Göncüoglu MC, Dirik K, Kozlu H (1997). Pre-Alpine and Alpine terranes in Turkey: explanatory notes to the terrane map of Turkey. Annales Geologiques des Pays Helleniques 37: 515-536.

Göncüoğlu MC, Turhan N, Şentürk K, Özcan A, Uysal Ş et al. (2000). A geotraverse across northwestern Turkey: tectonic units of the Central Sakarya region and their tectonic evolution. Geological Society of London, Special Publications 173: 139-161.

Göncüoglu MC, Gürsu S, Tekin UK, Köksal S (2008). New data on the evolution of the Neotethyan oceanic branches in Turkey: Late Jurassic ridge spreading in the Intra-Pontide branch. Ofioliti 33: 153-164.

Goncuoğlu MC, Sayit K, Tekin UK (2010). Oceanization of the northern Neotethys: geochemical evidence from ophiolitic mélange basalts within the Izmir–Ankara suture belt, NW Turkey. Lithos 116: 175-187.

Göncüoglu MC, Marroni M, Sayit K, Tekin UK, Ottria G et al. (2012). The Aylı Dağ ophiolite sequence (central Northern Turkey): a fragment of middle Jurassic oceanic lithosphere within the Intra-Pontide suture zone. Ofioliti 37: 77-92.

Göncüoglu MC, Marroni M, Pandolfi L, Ellero A, Ottria G et al. (2014). The Arkot Dağ Mélange in Araç area, central Turkey: Evidence of its origin within the geodynamic evolution of the Intra-Pontide suture zone. Journal of Asian Earth Sciences 85: 117-139.

Göncüoğlu MC, Tekin UK, Sayıt K, Bedi Y, Uzuncimen S (2015). Opening, evolution and closure of the Neotethyan oceanic branches in Anatolia as inferred by radiolarian research. Radiolaria 35: 88-90.

Göncüoğlu MC (2019). A review of the geology and geodynamic evolution of tectonic terranes in Turkey. In: Pirajno F, Ünlü T, Dönmez C, Bahadır Şahin, M. (editors). Modern Approaches in Solid Earth Sciences. 16: 19-72. Springer Nature.

Jolly WT, Lidiak EG, Dickin AP, Wu TW (1998). Geochemical diversity of Mesozoic island arc tectonic blocks in eastern Puerto Rico. Geological Society of America 322: 67-98.

Jolly WT, Lidiak EG, Dickin AP, Wu TW (2001). Secular geochemistry of central Puerto Rican island arc lavas: Constraints on Mesozoic tectonism in the eastern Greater Antilles. Journal of Petrology 42: 2197-2214.

Ludwig KR (2003). Isoplot 3.00. A Geochronological Toolkit for Microsoft Excel, vol. 4. Berkeley, California, USA: Berkeley Geochronology Center (70 pp.).

Marroni M, Göncüoğlu MC, Frassi C, Sayıt K, Pandolfi L et al. 2020. The Intra-Pontide ophiolites in Northern Turkey revisited: From birth to death of a Neotethyan oceanic domain. Geoscience Frontiers 11: 129-149.

Meschede M (1986). A method of discriminating between different types of mid-ocean ridge basalts and continental tholeiites with the Nb-Zr-Y diagram. Chemical Geology 56: 207-218.

Okay AI, Tuysuz O (1999). Tethyan sutures of northern Turkey. In: Durand B, Jolivet L, Horvath F, Seranne M (editors.), The Mediterranean Basins: Tertiary Extension within the Alpine Orogen. London, UK: Geological Society, Special Publications, 156: 475-515.

Okay AI, Göncüoğlu MC (2004). The Karakaya Complex: a review of data and concepts. Turkish Journal of Earth Sciences 13: 77-95.

Okay AI, Tüysüz O, Satır M, Altıner SÖ, Sherlock S et al. (2006). Cretaceous and Triassic subduction-accretion, high pressure-low temperature metamorphism, and continental growth in the Central Pontides, Turkey. Geological Society of America Bulletin, 118, 1247-1269.

Okay AI, Sunal G, Sherlock S, Altıner D, Tüysüz O et al. (2013). Early Cretaceous sedimentation and orogeny on the active margin of Eurasia: Southern Central Pontides, Turkey. Tectonics 32: 1247-1271.

Okay AI, Altiner D, Sunal G, Aygül M, Akdoğan R et al. (2018). Geological evolution of the Central Pontides. London, UK: Geological Society, Special Publications, 464: 33-67.

Ottria G, Pandolfi L, Catanzariti R, Da Prato S, Ellero A et al. (2017). Evolution of an Early Eocene pull-apart basin in the Central Pontides (Northern Turkey): New insights into the origin of the North Anatolian Shear Zone. Terra Nova 29: 392-400.

Özkan M, Çelik ÖF, Soycan H, Çörtük RM, Marzoli A (2020). The Middle Jurassic and Early Cretaceous basalt-radiolarian chert association from the Tekelidağ Mélange, eastern İzmir-Ankara-Erzincan suture zone (northern Turkey). Cretaceous Research: 107:104280

Parlak O, Çolakoğlu A, Dönmez C, Sayak H, Yıldırım N et al. (2012). Geochemistry and tectonic significance of ophiolites along the Ankara-Erzincan Suture Zone in northeastern Anatolia. In: Robertson AHF, Parlak O, Ünlügenç UC (editors.), 2012. London, UK: Geological Society, Special Publications, 372: 75-105.

Pearce JA, Cann JR (1973). Tectonic setting of basic volcanic rocks determined using trace element analyses. Earth and Planetary Science Letters 19: 290-300.

Pearce JA, Peate DW (1995). Tectonic implications of the composition of volcanic arc magmas. Annual Review of Earth and Planetary Sciences 23: 251-286.

Plank T, Langmuir CH (1998). The chemical composition of subducting sediment and its consequences for the crust and mantle. Chemical Geology 145: 325-394.

Robertson AHF, Dixon JE, Brown S, Collins A, Morris A et al. (1996). Alternative tectonic models for the Late Palaeozoic-Early Tertiary development of Tethys in the Eastern Mediterranean region. London, UK: Geological Society, Special Publications, 105: 239-263.

Rollinson H (1993). Using Geochemical data: Evaluation, Presentation, Interpretation. New York, NY, USA: Longman/Wyllie

Sayıt K, Göncüoğlu MC (2009). Geochemistry of mafic rocks of the Karakaya complex, Turkey: evidence for plume-involvement in the Paleotethyan extensional regime during the Middle and Late Triassic. International Journal of Earth Sciences 98: 157-185.

Sayit K, Tekin UK, Göncüoğlu MC (2011). Early-middle Carnian radiolarian cherts within the Eymir unit, Central Turkey: constraints for the age of the palaeotethyan Karakaya complex. Journal of Asian Earth Sciences 42: 398-407.

Sayıt K, Göncüoğlu MC (2013). Geodynamic evolution of the Karakaya Mélange Complex, Turkey: a review of geological and petrological constraints. Journal of Geodynamics 65: 56-65.

Sayit K, Marroni M, Göncüoğlu MC, Pandolfi L, Ellero A et al. (2016). Geological setting and geochemical signatures of the mafic rocks from the Intra-Pontide Suture Zone: implications for the geodynamic reconstruction of the Mesozoic Neotethys. International Journal of Earth Sciences 105: 39-64.

Sevin M, Uğuz MF (2011). Çankırı-G32 paftasına ait rapor, No: 148. Maden Tetkik ve Arama Genel Müdürlüğü, Ankara (in Turkish).

Sun SS, McDonough WF (1989). Chemical and isotopic systematics of oceanic basalts: implications for mantle composition and processes. London, UK: Geological Society, Special Publications, 42: 313-345.

Şengör AMC, Yılmaz Y (1981). Tethyan evolution of Turkey: A plate tectonic approach. Tectonophysics 75: 181-241.

Taylor SR, McLennan SM (1995). The geochemical evolution of the continental crust. Reviews of Geophysics 33: 241-265.

Tekin UK, Göncüoğlu MC, Pandolfi L, Marroni M (2012). Middle Late Triassic radiolarian cherts from the Arkotdağ melange in northern Turkey: implications for the life span of the northern Neotethyan branch. Geodinamica Acta 25: 305-319.

Topuz G, Okay AI, Schwarz WH, Sunal G, Altherr R et al. (2018). A middle Permian ophiolite fragment in Late Triassic greenschist- to blueschist-facies rocks in NW Turkey: An earlier pulse of suprasubduction-zone ophiolite formation in the Tethyan belt. Lithos 300: 121-135.

Tüysüz O (1990). Tectonic evolution of a part of the Tethyside orogenic collage: the Kargi Massif, northern Turkey. Tectonics 9: 141-160.

Tüysüz O (1993). Karadeniz'den Orta Anadolu'ya bir jeotravers: Kuzey Neo-Tetisin tektonik evrimi: Türkiye Petrol Jeologları Derneği Bülteni 5: 1-33 (in Turkish).

Tüysüz O, Dellaloğlu AA, Terzioğlu N (1995). A magmatic belt within the Neo-Tethyan zone and its role in the tectonic evolution of northern Turkey. Tectonophysics 243: 173-191.

Ustaömer T, Robertson AHF (1997). Tectonic-sedimentary evolution of the north Tethyan margin in the Central Pontides of northern Turkey. AAPG Mem 68: 255-290.

Uğuz MF, Sevin M, Duru M (2002). Sinop sheet in the Geological map series of Turkey, scale 1: 500 000. Maden Tetkik ve Arama Genel Müdürlüğü, Ankara.

Winchester JA, Floyd PA (1977). Geochemical discrimination of different magma series and their differentiation products using immobile elements. Chemical geology 20: 325-343.

Wood DA, Gibson IL, Thompson RN (1976). Elemental mobility during zeolite facies metamorphism of the Tertiary basalts of eastern Iceland. Contributions to Mineralogy and Petrology 55: 241-254.

Yalınız MK, Floyd PA, Göncüoğlu MC (1996). Supra-subduction zone ophiolites of central Anatolia: geochemical evidence from the Sarıkaman ophiolite, Aksaray, Turkey. Mineralogical Magazine 60: 697-710.

Yılmaz Y, Tüysüz O (1988). Kargı masifi ve dolaylarında Mezozoyik tektonik birliklerin düzenlemeleri sorununa bir yaklaşım. Turkish Association of Petroleum Geologists Bulletin 1: 73-86 (in Turkish).

Yılmaz Y, Tüysüz O, Yiğitbaş E, Genç ŞC, Şengör AMC (1997). Geology and tectonic evolution of the pontides. In: Robinson, A.G. (editor). Regional and Petroleum Geology of the Black Sea and Surrounding Region: American Association of Petroleum Geologists Memoir 68: 183-226.

Pearce JA, Stern RJ, Bloomer SH, Fryer P (2005). Geochemical mapping of the Mariana arc-basin system: Implications for the nature and distribution of subduction components. Geochem Geophys Geosyst. doi:10.1029/2004GC000895